UNIVERSITY OF CALIFORNIA SAN DIEGO

Helium and carbon systematics of northern Baja California: an assessment of geothermal resources

A Thesis submitted in partial satisfaction of the requirements
for the degree of Master of Science

in

Earth Sciences

by

Cristian Enrique Virrueta

Committee in charge:

Paterno Castillo, Chair
Justin Kulongoski
Peter Lonsdale

2018

The Thesis of Cristian Enrique Virrueta is approved and it is acceptable in quality and form for publication on microfilm and electronically:

_____

_____

_____

Chair

University of California San Diego

2018

DEDICATION

This thesis is dedicated to my wonderful family, my wife, father, older brother, and younger sister. Without their constant encouragement and patience with me throughout the duration of this project, its completion would not have been possible. I dedicate this study to my Late Mother, Margarita Virrueta (1964 – 2015), who throughout her short lifetime etched in the walls of my heart the importance of love, family, and education.

EPIGRAPH

We cannot seek achievement for ourselves and forget about progress and prosperity for our community… Our ambitions must be broad enough to include the aspirations and needs of others, for their sakes and for our own.

César Chávez

TABLE OF CONTENTS

LIST OF FIGURES

LIST OF TABLES

ACKNOWLEDGEMENTS

This manuscript would be far from complete without thanking the following people for their support throughout this project. I thank my advisor, Dr. Paterno Castillo, for providing me with the opportunity to pursue my graduate degree and always being available for discussions. I thank Dr. Justin Kulongoski and Dr. Peter Lonsdale for standing on my committee and providing suggestions for my thesis. I am indebted to Dr. Raquel Negrete-Aranda, Dr. Ronald Spelz, and their colleagues for their unwavering support and contribution in executing the fieldwork, providing feedback on my thesis, and constant encouragement and hospitality. I would also like to extend my gratitude to Michael Land at the U.S. Geological Survey, Dr. Andrew Dickson and his lab, Bruce Deck, Brian House, and Keith Blackmon for helping me in conducting all the relevant analyses for this project. Lastly, I thank Dr. David Hilton, who has influenced not only my graduate studies, but also my young adult life. He has instilled in me by example, a strong sense of discipline, integrity, and a passion for science for which I am eternally grateful. David's great scientific mind and adventurous spirit will be dearly missed. This project was in part possible from funds derived from project No. 401/1/C/142/18 from the Universidad Autonoma de Baja California, awarded to Ronald Spelz and funding for Raquel Negrete-Aranda was provided by CATEDRAS CONACYT Project 2074 and CICESE Internal Project 644149.

ABSTRACT OF THE THESIS

Helium and carbon systematics of northern Baja California: an assessment of geothermal resources

by

Cristian Enrique Virrueta

Master of Science in Earth Sciences

University of California San Diego 2018

Professor Paterno Castillo, Chair

The Baja California Peninsula represents an area of anomalous heat flow evidenced by an abundance of subaerial geothermal manifestations and submarine hydrothermal vents. We report helium and carbon isotopic and relative abundance data from 13 geothermal springs throughout northern Baja California. Results of this study reveal $^{3}He/^{4}He$ values ranging from 0.11 to 1.74 R_A (where R_A = air $^{3}He/^{4}He$) and concentrations of ^{4}He, corrected for air contamination, vary from 0.284 to 1207 ($\times 10^{-6}$) cm^3 STP/gH_2O. Carbon isotopes ($\delta^{13}CO_2$) vary between -19.39 to +9.08‰ (vs. PDB) and $CO_2/^{3}He$ values vary over several orders of magnitude (2.02×10^{5} to 1.06×10^{13}). $^{3}He/^{4}He$ values are attributed to mixing between mantle-derived helium and a radiogenic

component derived from the crust. The highest $^{3}He/^{4}He$ values lie toward the east in the Gulf Extensional Province (GEP), are proximal to spreading centers, and are in agreement with low mantle velocity zones observed in recent tomography studies. Variable $\delta^{13}CO_2$ and $CO_2/^{3}He$ values at these localities are consistent with phase separation and/or calcite precipitation in shallow-level hydrothermal systems. Both processes result in CO_2 loss which exacerbates the effects of contamination by crustal gases. The value of the majority of samples in the present study lies with discerning the potentially complicating effects of degassing and/or crustal contamination on the resulting CO_2 record. Ultimately, the Puertecitos and Punta Estrella regions can be considered a promising geothermal prospect with a potential to satisfy the increasing energy demands of the Baja California Peninsula.

1. INTRODUCTION

The Baja California Peninsula and the Gulf of California have long been identified as areas with high geothermal potential (Quijano and Gutierrez-Negrin, 2005). Currently, the country of Mexico has a net geothermal-electric capacity of 958 MW, produced by four geothermal fields: Cerro Prieto, Los Azufres, Los Humeros, and Las Tres Virgenes (Flores-Armenta and Gutierrez-Negrin, 2011). However, there is a pressing need to identify and evaluate geothermal areas in the region for future development. A geothermal survey of the northern peninsula, targeting subaerial geothermal manifestations, will greatly enhance the assessment of the geothermal potential of Baja California. In addition, a geochemical perspective will lead to a better understanding of the thermal structure and the magmatic evolution of this region.

Prior studies (e.g. Vidal, 1982, Welhan et al., 1988, and Forrest et al., 2005) have identified multiple geothermal springs throughout Baja California, and some of these include some small-scale helium and carbon isotopic investigation. Helium is a sensitive tracer of mantle-derived fluids, and its distribution throughout Baja California allows for the differentiation between various mantle and crustal sources of volatiles (Hilton, 1996; Kulongoski and Hilton, 2011). Primordial helium (^{3}He) is a rare isotope that has been primarily stored in the Earth's mantle since accretion, and is relatively, enriched in magmas derived through partial melting of the mantle. In contrast, the Earth's crust is enriched in radiogenic helium (^{4}He) due to the radioactive decay of uranium and thorium. Thus, the ratio between ^{3}He and ^{4}He in geothermal fluids can indicate the origin (i.e., mantle vs. crust). Fluids originating in the crust have low ratios of ^{3}He to ^{4}He – usually

0.02 to 0.05 R_A (Andrews, 1985) where R_A is the standard atmospheric $^3He/^4He$ ratio ($1.38x10^{-6}$; Clarke et al., 1976). Mantle-derived helium has a higher $^3He/^4He$ ratio, with mantle-derived mid-ocean ridge basalts (MORB) having values of 8 R_A. Mantle-derived helium and high CO_2 concentrations have been linked to volcanic arcs, hotspots and mid-ocean ridges, areas known for high heat flow and mantle partial melting (Hilton and Porcelli, 2003). Furthermore, in the absence of magmatic activity, crustal faulting plays an important role in the transfer of mantle-derived volatiles through the crust (Hilton, 2007). Quantifying the CO_2 flux, coupled together with helium ($CO_2/^3He$ ratio), as well as the $\delta^{13}C$ (CO_2), can all be utilized as sensitive indicators of the provenance of carbon and successfully discriminate mantle reservoir signatures from those of the crust (Lollar et al., 1997).

Here, we quantify the heat characteristics of northern Baja California utilizing chemical and isotopic analyses of 13 geothermal springs located throughout this area. By targeting helium isotopes, gas chemistry, and water chemistry, we identified regions of mantle degassing with helium and carbon isotopes. Coupled with existing geophysical data, a better understanding of the northern Baja California mantle structure has been gained.

2. GEOLOGIC AND TECTONIC BACKGROUND

2.1 Tectonic History

Baja California is a 1200 km long peninsula separated from mainland Mexico by the Gulf of California. The Gulf is situated along a plate boundary between the Pacific and North American plates and is part of a large rift, dominated by right lateral (dextral) faults and active spreading centers that form the San Andreas-Gulf of California fault system (Figure 1). Offshore, towards the west, Baja California is bounded by right lateral strike-slip faults such as the Tosco-Abreojos and San Clemente-San Isidro faults.

Baja California is primarily composed of four main structural provinces: (1) the Gulf Extensional Province, present along the eastern margin, (2) the unextended central and western portion of the peninsula, (3) the Transpeninsular Strike-slip Province, which encompasses the northwestern part of the peninsula, and (4) the sheared continental borderland west of Baja California (Figure 6). The Gulf Extensional Province is constrained to the west by the Main Gulf Escarpment, a north-south striking and east dipping normal fault, and to the east by the Sierra Madre Occidental located in mainland Mexico (Seiler et al., 2010). This province is a zone characterized by basin and range-like extension and topography. In the Main Gulf Escarpment, defined by the northern Sierra Juárez, the central and southern Sierra San Pedro Mártir rises steeply to a maximum elevation of 1800 meters (Axen 1995).

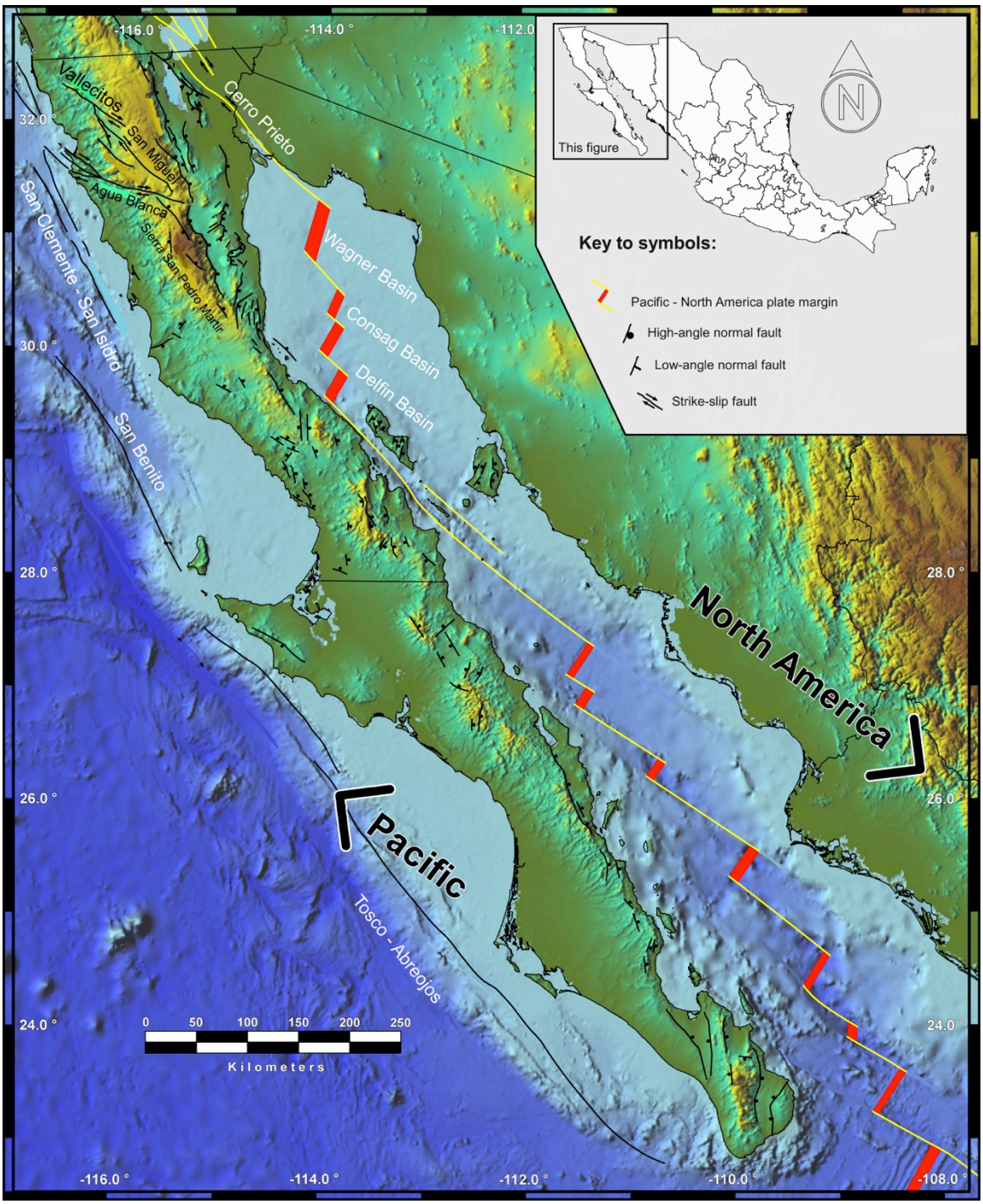

Figure 1: Regional tectonic map of the Baja California Peninsula and the Gulf of California. Faults, mountain ranges, and other features are also labeled. Figure modified from Spelz et al., 2017.

The Transpeninsular Strike-slip Province is dominated by active faults that diverge westward from the main gulf axis. The WNW-striking Agua Blanca fault and the NW-striking San Miguel-Vallecitos fault system accumulate strain with a combined slip rate of 4 to 8 mm per year (Seiler et al., 2010). The Agua Blanca fault is 130 km long and extends from the Punta Banda Peninsula near Ensenada to San Matias Pass on the Main Gulf Escarpment (Suarez-Vidal et al., 2007). The San Miguel-Vallecitos fault system is comprised of four faults: San Miguel, Vallecitos, Calabazas, and Tres Hermanos.

Prior to the formation of the Gulf of California, the North American continental margin in western Mexico had been a convergent boundary for some time. The subduction of the eastward-moving Farallon Plate beneath the western edge of the North American Plate generated a volcanic arc along the Sierra Madre Occidental in early Oligocene to early Miocene time (~34-23 Ma) (Umhoeher et al., 2000; Castillo, 2008). Arc volcanism migrated west during the middle Miocene (~15 Ma) and formed the Comondú volcanic arc in ancestral Baja California. The central region of the Farallon Plate subducted as the leading segment of the East Pacific Rise (EPR) met with the North American Plate, ~25 Ma ago in central California, and ~15 Ma ago in northern Mexico (Lonsdale, 1989). It was the collision of the EPR with the west coast of North America that created the modern San Andreas Fault system. Today, the Mendocino Triple Junction marks the northern limit of this transform/divergent boundary system, and the Rivera Triple Junction marks the southern limit (Wallace, 1990).

At 15 Ma, the EPR was obliquely converging with the trench along the continental margin. As the rise neared the trench, the plate fragmented into independently moving slabs such as the Guadalupe and Magdalena microplates and was ultimately

captured by the Pacific plate (Tian et al., 2011). North of the Shirley Fracture Zone, at ~12.5 Ma, spreading and subduction ceased, with the Magdalena microplate capture continuing until 8 to 7 Ma during which the spreading axis broke into short segments and rotated clockwise (Michaud et al., 2006; Calmus et al., 2011). The boundary between the Pacific and North American plates was located along the Tosco-Abreojos and San Benito fault zones from 8 to 7 Ma until ~6 Ma, when the transtensional regime in the Gulf of California became established. Since 5 Ma, the EPR propagated northwards, forming several extensional centers connected by transform faults, which extend up to the San Andreas Fault system (Lonsdale, 1989). From this point in time, the peninsula represents a continental block that was captured by the Pacific Plate and is currently moving away from the North America mainland.

2.2 Volcanic History

During its Cenozoic tectonic evolution, Baja California has been the locus of numerous volcanic events involving the eruption of calc-alkaline volcanics, tholeiites, adakites and magnesian andesites. Volcanic activity has occurred along the eastern margin of Baja California since the Oligocene, with calc-alkaline arc volcanism occurring along what is now the eastern coast of the peninsula (Negrete-Aranda et al., 2013). During middle Miocene time, a transform fault system developed between the Pacific and North American plates, shifting the convergent margin of North America to a transform plate margin. Despite the cessation of subduction, volcanism has continued up to Quartenary times and is manifested in several monogenetic volcanic fields located west of the extinct volcanic arc. Focusing on northern Baja California, the most recent

volcanic activity in the region has occurred in five volcanic centers: Cerro Prieto, San Quintín, Puertecitos, Jaraguay, and San Borja. Cerro Prieto is the name of a Quaternary, isolated, and monogenetic volcano northwest of the Cerro Prieto Geothermal Field. The volcano rises 260 meters above sea level and is located in the northern peninsula, approximately 35 km south of the city of Mexicali (Lindsay and Hample, 1998). The dacitic lavas are the only surface evidence of volcanic activity in the Cerro Prieto geothermal field, which is the largest field in exploitation in Mexico. Paleomagnetic data indicates that the volcanic activity occurred between 100,000 and 10,000 years ago (De Boer, 1980).

The San Quintín volcanic field lies along the Pacific coast of northern Baja California, approximately 260 km south of the U.S.-Mexico border. It is primarily composed of monogenetic Quaternary lavas with rocks composed of intraplate basaltic composition and peridotitic and granulitic xenoliths (Luhr et al., 1995).

The Puertecitos volcanic province is located along the northeastern margin of the Peninsula and consists of andesitic lava flows and rhyolitic pyroclastic flows with ages of 3.2 to 2.7 Ma (Martín-Barajas et al., 1995). Near the coast, the volcanic province is cut by high-angle normal faults, such as the San Perdo Martír fault, due to the region's prevailing extensional tectonics.

The Jaraguay and San Borja volcanic fields are located in the central part of the peninsula. They include lava flows and hundreds of scoria cones with ages from 5 to 0.5 Ma (Pallares et al., 2008; Negrete-Aranda et al., 2010).

The higher than average heat flow setting of the peninsula coupled with volcanic and tectonic activity, has produced conditions for the occurrence of numerous geothermal

areas along the coasts (Vidal et al., 1981). The fault planes act as conduits and allow meteoric and/or seawater to penetrate deep into the crust and be heated by the anomalously high geothermal gradient of the region. The geothermal manifestations investigated in this study are mostly subaerial hot and warm springs, water wells, and springs located off shore (Figure 2).

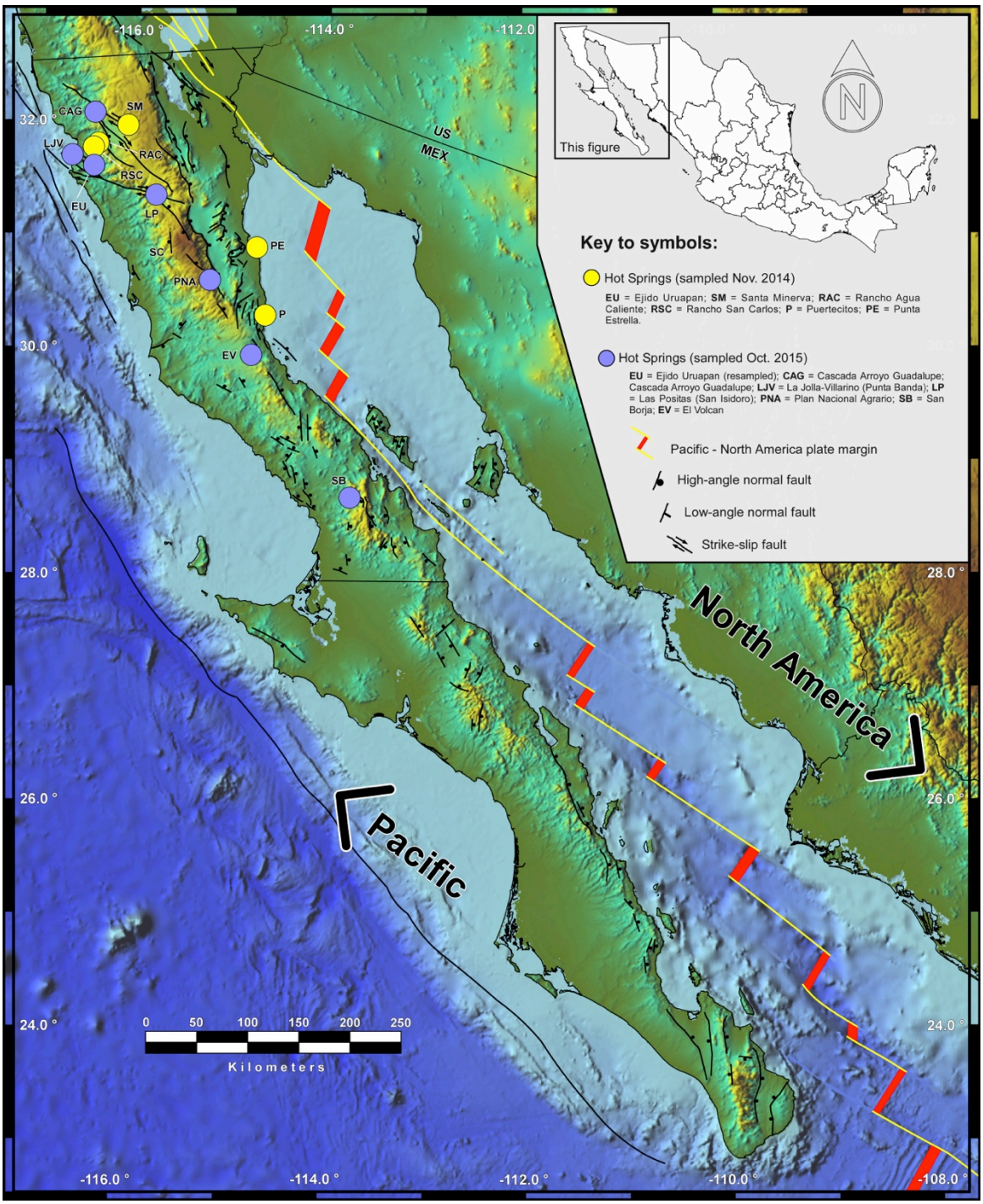

Figure 2: Map of the study area illustrating sample localities (yellow circles = sampled in 2014, purple circles = sampled in 2015). Figure modified from Spelz et al., 2017.

3. FIELD COLLECTION AND ANALYTICAL METHODS

Groundwater and geothermal samples were collected from 13 different localities throughout northern Baja California peninsula during the span of three sampling campaigns in 2001, 2014, and 2015. A total of 28 samples (including duplicates and triplicates) were collected: 2 in 2001, 12 in 2014, and 14 in 2015. A total of 15 gas and 13 water samples were included in this study.

3.1 Groundwater Sampling for Dissolved Gases

Standard sampling protocols were adopted for the collection of volatiles from bubbling hot springs (following Hilton et al., 2002). Evacuated 1720 glass flasks and 3/8-inch copper tubes were utilized to collect samples. The use of copper tubes preserves the integrity of the sample even after significant durations of storage due to the low permeability of copper to helium (Weiss, 1968). Gases bubbling into hot springs are sampled by placing an inverted funnel at the bottom of the spring. A Tygon tube links the funnel to one end of the copper tube or glass flask inlet. A second Tygon tube is attached to the other end of the copper tube or flask outlet, allowing the discharge water or gas to flow through the tube assembly. After flushing the system to avoid air contamination, the copper tube is crimped shut using refrigeration clamps on both ends of the tube forming an air-tight seal. In the case of the glass flasks, the outlet Tygon tube is clamped shut and the valve to the flask is opened to the vacuum and then closed thereby trapping the sample into the flask.

3.2 Groundwater Sampling for Water Chemistry

At each locality, hot spring waters were collected in three 125 mL screw-cap bottles for alkalinity, cation, and anion analyses. All waters are filtered using a syringe equipped with a 0.45 µm filter attachment. Bottles for alkalinity measurement were poisoned using $HgCl_2$ (Dickson et al., 2003). Bottles for anion and cation measurement were rinsed with native water three times and filled leaving a small headspace, with cation bottles later acidified using a few drops of HNO_3. The temperature, pH, and total dissolved solids of each sampling site were obtained using a YSI Professional Plus multi-meter. Waters were collected for water chemistry only during the 2014 and 2015 campaigns.

3.3 Fluid Extraction, Noble Gas Separation, Quadrupole Mass Spectrometer System (FENG-QMS)

Samples were processed using the Fluid Extraction, Noble Gas Separation, Quadrupole Mass-Spectrometer System (FENG-QMS) at Scripps Institution of Oceanography (Kulongoski and Hilton, 2002). This system extracts water and gas from a variety of sampling media (copper tubes, flasks, etc.), removes water vapor and reactive gases, and isolates noble gases for mass spectrometric analyses. The extraction line is comprised of three sections: a sample release section, gas separation section, and gas measurement section. In the sample release section, the sample is mounted vertically onto the line and opened. With water samples, a bulb containing phosphorous pentoxide is attached to the line to drive CO_2 out of solution. Water vapor is isolated using a 1720 glass water trap submerged in an (-78°C) acetone and dry ice mixture. Thereafter, the

CO_2 is condensed onto a stainless steel U-trap submerged in (-196°C) liquid nitrogen. At this stage, the remaining gases enter the gas preparation section, where an aliquot of gas is collected in 1/4-inch copper tube for further purification and nitrogen isotopic measurement. Next, helium and neon are isolated using an activated charcoal finger submerged in liquid nitrogen to adsorb argon, krypton, and xenon. Then, residual gas is exposed to a hot (700°C) titanium getter to remove nitrogen and other reactive gases. A split of helium and neon is taken in a 1/4-inch copper tube for isotopic measurement on a MAP 215 noble gas mass spectrometer. The residual helium and neon is transferred to the gas measurement section where a quadrupole mass spectrometer (QMS) estimates the helium and neon abundance. Lastly, the CO_2 is released from the U-trap by removing the liquid nitrogen and condensing it to a 1/4-inch copper tube. The CO_2 is then transferred to a separate line for further purification prior to $\delta^{13}C$ analysis.

3.4 Magnetic Sector Mass Spectrometer (MAP-215)

The helium and neon aliquot taken from the FENG-QMS line is processed through a noble gas mass spectrometer (MAP-215) to determine helium and neon abundance as well as the $^3He/^4He$ ratio. The gas is inlet from the breakseal to the preparation line where charcoal fingers held at liquid nitrogen temperature (-196°C) and a titanium getter (700°C) purify the gas. The helium and neon are condensed using a cryogenic trap cooled to 15K and released sequentially by increasing the temperature to 35K and 90K for helium and neon, respectively. Once inlet into the MAP-215, helium and neon peak intensities are measured and the $^3He/^4He$ ratio of the sample is normalized to standards of atmospheric air.

3.5 CO_2 Clean Up Line and Isotope Ratio Mass Spectrometer (IRMS)

The CO_2 fraction previously isolated from the extraction line is processed in a Pyrex glass preparation line. Using a variable temperature trap, the CO_2 and any undesirable gases (e.g., SO_2) are separated and the total amount of CO_2 is quantified in a calibrated volume using a capacitance manometer. Thereafter, the purified CO_2 is condensed into a Pyrex glass tube and transferred to a Thermo Finnigan Delta XP_{plus} isotope ratio mass spectrometer for carbon isotope ($\delta^{13}C$) measurement. Values are reported relative to the international standard Vienna Pee Dee Belemnite (V-PDB) and have a precision of less than 1‰ (Barry et al., 2013).

3.6 Water Chemistry and Total Alkalinity

The concentrations of major anions (F^-, Cl^-, NO_3^-, and SO_4^{-2}) and cations (Ca^{+2}, Mg^{+2}, Na^+, and K^+) were ascertained using a Metrohm 850 Professional Ion Chromatograph operated by the California Water Science Center (part of the U.S. Geological Survey) in San Diego, California. The anion and cation analyses were performed following the protocols outlined in the EPA Method 300.0 (U.S. Environmental Protection Agency, 1993) and Metrohm's analysis and instrument monograph (Bruttel and Seifert, 2007). The ion chromatograph is calibrated with National Water Quality Laboratory (NWQL) blank water and stock solutions of varying dilutions (1:5 through 1:1000) utilizing a multi-ion standard solution containing the analytes of interest. A calibration curve is formulated by plotting peak area versus known concentrations of blank water and working standards. After conducting a simple regression analysis and achieving a correlation coefficient of 0.995 or greater, the

unknown sample analysis is carried out. NWQL blank water, standard reference samples with known concentrations, and working standards are evaluated in conjunction with our unknown sample analyses to ensure instrument accuracy and precision. When analyte concentrations exceed the calibration range, samples are diluted accordingly to match standards and ensure reproducibility.

Total alkalinity was determined using a two-stage open-cell titration technique as described in Dickson et al., (2003) at the Scripps Institutions of Oceanography. Samples were first acidified to a pH between 3.5 and 4.0 using HCl and titrated until the solution reached an approximate pH of 3.0. Utilizing a least-squared procedure, the total alkalinity and equivalence point were calculated. Normal laboratory quality control samples were run in conjunction with unknown samples being analyzed. For total alkalinity, seawater reference materials were used. In addition, tap water was used for precision measurements because of its similarity in composition to the groundwaters being analyzed. Because of the source of the water, it was not uncommon to find sediment in the sample bottles that made its way to the titration cell. It is possible that this could have had an effect on the electrode during titrations, so tap water was measured to ensure normal electrode responses and high precision.

4. RESULTS

The helium and carbon results of all samples are presented in Table 1. Table 2 contains the end-member contributions from each sample, and these are graphically presented in Figure 3. Lastly, major ion water chemistry is presented in Table 3, with Figure 4 containing a graphical representation of the water chemistry in the form of a Piper diagram, a useful way to detect general trends and define hydrochemical facies.

4.1 Helium Isotope Ratios ($^3He/^4He$)

The measured $^3He/^4He$ ratios as well as the air-corrected $^3He/^4He$ ratios are reported in Table 1 in the R_A notation. The $^3He/^4He$ in the atmosphere is 1.38×10^{-6} and is represented by R_A (Clarke et al., 1976). Corrections for atmospheric contamination were completed utilizing the following equation (Craig et al., 1978; Hilton, 1996):

$$R_C/R_A = [(R_M/R_A)X - 1]/(X - 1)$$

where R_C/R_A is the air-corrected helium ratio and X is the air-normalized $^4He/^{20}Ne$ ratio defined as:

$$X = \left[\left(^4He/^{20}Ne\right)_M/\left(^4He/^{20}Ne\right)_A\right](\beta_{Ne}/\beta_{He})$$

where $(^4He/^{20}Ne)_M$ is the measured ratio, $(^4He/^{20}Ne)_A$ is the ratio of air, and β is the Bunsen solubility coefficient calculated for Ne and He. A coefficient of 1.22 was utilized assuming an average recharge temperature of 15°C (Weiss, 1971; Ozima and Podosek, 1983).

Table 1: Helium and carbon isotope and relative abundance characteristics from Baja California.

Location	Sample ID	Sample Type[a]	Latitude	Longitude	T(°C)/pH	$^3He/^4He$ R_M/R_A[b]	X[c]	$^3He/^4He$ R_C/R_A[d]	$CO_2/^3He$ ($x10^9$)	$\delta^{13}C$ (CO_2) (‰)VPDB	$[^4He]_C$ cm^3STP	$[^4He]_C$ cm^3STP/gH_2O ($x10^{-6}$)[e]
Cascada Arroyo Guadalupe	**BAJA-21**	**G**	**N 32°03′42″**	**W 116°15′54″**	**52/8.5**	**0.40**	**2114**	**0.40 ± 0.02**	**0.000311**	**-16.69**	**2.95E-02**	**n.d.**
Santa Minerva	BAJA-12	G	N 31°59′58″	W 116°05′39″	58.3/9.26	0.11	1500	0.11 ± 0.01	0.000815	-10.83	4.89E-02	n.d.
	BAJA-14	**G**				**0.11**	**1880**	**0.11 ± 0.01**	**0.000202**	**-19.39**	**5.79E-02**	**n.d.**
Rancho Agua Caliente	BAJA-11	W	N 31°49′52″	W 116°23′17″	43.2/9.29	0.33	58.6	0.32 ± 0.02	3.98	6.48	2.13E-04	5.50
	BAJA-20	**W**				**0.34**	**188**	**0.33 ± 0.02**	**2.91**	**7.20**	**2.93E-04**	**7.36**
Rancho San Carlos	BAJA-07	W	N 31°47′43″	W 116°26′05″	41.3/9.22	0.24	187	0.24 ± 0.01	4.16	4.80	2.89E-04	7.28
	BAJA-17	**W**				**0.24**	**195**	**0.24 ± 0.01**	**3.94**	**3.74**	**2.61E-04**	**6.43**
La Jolla - Villarino	**BAJA-22**	**G**	**N 31°43′09″**	**W 116°39′43″**	**63.6/8**	**0.22**	**932**	**0.22 ± 0.01**	**0.344**	**-14.24**	**5.41E-02**	**n.d.**
	BAJA-23	G				0.22	246	0.22 ± 0.01	1.22	-13.21	3.84E-03	n.d.
Ejido Uruapan	BAJA-01	W	N 31°37′58″	W 116°26′05″	55.3/9.21	0.62	94.9	0.59 ± 0.03	2.53	9.08	1.26E-03	3.19
	BAJA-06	W				0.65	130	0.65 ± 0.03	1.44	7.94	2.06E-04	5.29
Ejido Uruapan (re-sample)	**BAJA-24**	**G**	**N 31°37′58″**	**W 116°26′04″**	**57.7/9**	**0.55**	**517**	**0.55 ± 0.02**	**2.22**	**-4.47**	**9.19E-03**	**n.d.**
Las Positas	**BAJA-25**	**G**	**N 31°23′18″**	**W 115°47′01″**	**38.2/8.5**	**0.55**	**933**	**0.55 ± 0.02**	**0.000437**	**-14.42**	**1.65E-02**	**n.d.**
Punta Estrella	**BAJA-16**	**G**	**N 30°56′40″**	**W 114°44′01″**	**31.1/5.91**	**1.13**	**1160**	**1.13 ± 0.05**	**3.78**	**-3.22**	**3.92E-03**	**n.d.**
	BAJA-19	G				0.95	6.27	0.94 ± 0.06	2.61	-3.43	5.07E-04	n.d.
Plan Nacional Agrario	**BAJA-26**	**G**	**N 30°38′51″**	**W 115°12′27″**	**64.1/9**	**0.30**	**2382**	**0.30 ± 0.01**	**0.00219**	**-12.60**	**1.17E-01**	**n.d.**
	BAJA-27	G				0.26	41.6	0.25 ± 0.02	0.0139	-9.86	1.06E-03	n.d.
	BAJA-28	G				0.24	1747	0.24 ± 0.02	0.000788	-17.38	2.80E-02	n.d.
Puertecitos	BAJA-15	W	N 30°20′46″	W 114°38′10″	61.2/6.66	1.69	21.1	1.73 ± 0.07	2.90	-1.11	7.47E-05	2.02
	BAJA-18	**W**				**1.73**	**87.5**	**1.74 ± 0.04**	**14.1**	**-0.89**	**1.31E-04**	**3.13**
El Volcan-1	BAJA-29	G	N 29°59′33″	W 114°46′15″	23.4/6.5	0.94	1.21	0.87 ± 0.03	107.3	-9.05	4.50E-05	n.d.
	BAJA-30	G				0.68	1.68	0.61 ± 0.05	3257	-9.06	3.88E-06	n.d.
El Volcan-2	**BAJA-31**	**W**				**1.16**	**4.62**	**1.31 ± 0.09**	**10620**	**-5.72**	**9.86E-07**	**0.284**
San Borja	**BAJA-32**	**W**	**N 28°44′25″**	**W 113°45′07″**	**35.7/9**	**0.38**	**535**	**0.37 ± 0.02**	**0.0447**	**-12.46**	**2.64E-02**	**1207**
	BAJA-33	W				0.43	150	0.43 ± 0.02	0.00362	-13.13	4.07E-03	1136
	BAJA-34	G				0.59	8.83	0.55 ± 0.03	0.0574	-17.62	2.03E-04	n.d.
Ensenada	ENS-1	W	n.d.	n.d.	n.d.	0.55	447	0.55 ± 0.01	0.976	n.d.	n.d.	8.86
	ENS-2	**W**				**0.57**	**387**	**0.56 ± 0.01**	**0.926**	**-17.20**	**n.d.**	**7.81**

[a] Abbreviations (G) = Gas sample, (W) = Water sample

[b] R_M/R_A is measured $^3He/^4He$ ratio divided by the $^3He/^4He$ in air ($1.38x10^{-6}$).

[c] $X = (^4He/^{20}Ne)measured/(^4He/^{20}Ne)air \times \beta Ne/\beta He$ and β represents the Bunsen coefficient from (Weiss, 1971) assuming a groundwater recharge temperature of 15°C.

[d] R_C/R_A is the air-corrected He isotope ratio = $[(R_M/R_A)X-1]/(X-1)$.

[e] Dissolved He concentrations are air-corrected where $[He]_c = ([He]_m \times (X-1))/X$.

n.d. = not determined.

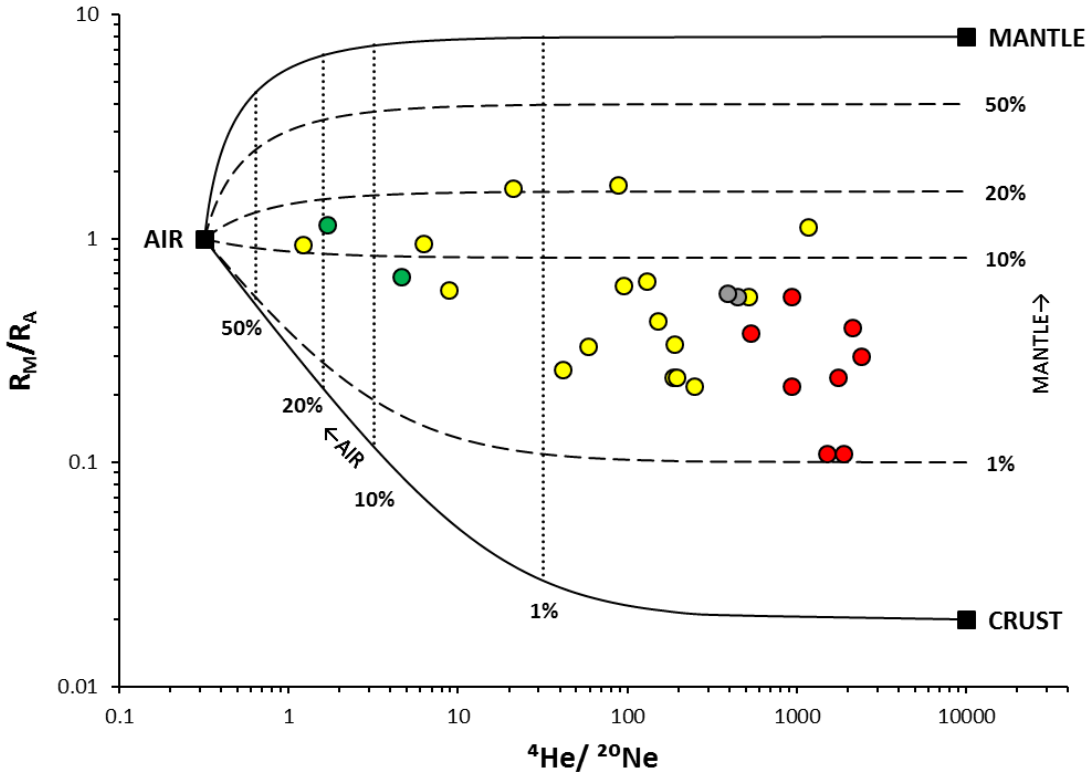

Figure 3: Plot of measured He isotopes versus solubility-corrected, air normalized He/Ne ratio (X) to assess the integrity of the He isotopes results. Curves represent mixing between air-saturated water (1 R_A, X=1), MORB (8 R_A), and crust (0.02 R_A).

Figure 3 illustrates an A-M-C plot, where the measured $^3He/^4He$ ratio and the $^4He/^{20}Ne$ ratio are utilized to estimate the degree of air contamination and/or mantle-derived and crustal helium contributions (Sano and Wakita, 1985). On the x-axis, a low X value results in greater corrections to the measured $^3He/^4He$ ratio, representing a larger input of air. Table 2 presents mantle, air, and crustal values calculated with the following equations (Sano and Wakita, 1985):

$$\left(^3He/\ ^4He\right)_O = f_M\left(^3He/\ ^4He\right)_M + f_A\left(^3He/\ ^4He\right)_A + f_C\left(^3He/\ ^4He\right)_C$$

$$1/\left(^4He/^{20}Ne\right)_O = f_M\left(^4He/^{20}Ne\right)_M + f_A\left(^4He/^{20}Ne\right)_A + f_C\left(^4He/^{20}Ne\right)_C$$

$$f_M + f_A + f_C = 1$$

Table 2: Calculation of mantle, air, and crustal helium contributions (in %), based on equations described above.

Location	Name	Mantle %	Air %	Crust %
CAG	BAJA-21	4.76	0.01	95.23
SM	BAJA-12	1.13	0.02	98.85
	BAJA-14	1.13	0.01	98.86
RAC	BAJA-11	3.82	0.54	95.64
	BAJA-20	3.99	0.17	95.84
RSC	BAJA-07	2.74	0.17	97.10
	BAJA-17	2.74	0.16	97.10
LJ-V	BAJA-22	2.50	0.03	97.47
	BAJA-23	2.49	0.13	97.38
EU	BAJA-01	7.48	0.33	92.19
	BAJA-06	7.86	0.24	91.89
EU resample	BAJA-24	6.63	0.06	93.31
LP	BAJA-25	6.64	0.02	93.33
PE	BAJA-16	13.91	0.02	86.07
	BAJA-19	11.03	5.10	83.87
PNA	BAJA-26	3.51	0.01	96.48
	BAJA-27	2.93	0.63	96.44
	BAJA-28	2.76	0.01	97.23
P	BAJA-15	20.74	1.51	77.75
	BAJA-18	21.38	0.36	78.25
EV-1	BAJA-29	8.28	26.44	65.27
	BAJA-30	7.42	6.92	85.66
EV-2	BAJA-31	11.95	19.05	69.01
SB	BAJA-32	4.50	0.06	95.44
	BAJA-33	5.11	0.21	94.68
	BAJA-34	6.70	3.62	89.68
ENS	ENS-1	6.63	0.07	93.30
	ENS-2	6.88	0.08	93.04

where the subscripts O, M, and C represent the observed, mantle, atmospheric, and crustal $^3He/^4He$ and $^4He/^{20}Ne$ ratios respectively, and f stands for the fraction of each end-member. The end-members for mantle, atmosphere, and crust are 8 ± 1 R_A (Graham 2002), 1 R_A, and 0.02 R_A (Andrews, 1985) respectively.

All samples, including duplicates, range from 0.11 R_A (Santa Minerva) and 1.74 R_A (Puertecitos), well below typical values of Mid-Ocean Ridge Basalts (MORB = 8 ± 1 R_A) and the Global Arc Average (GAA = 5.4 R_A; Hilton et al., 2002). However, all samples plot above typical values for radiogenic helium with a minimum 1% mantle contribution. At all localities, duplicate samples were taken and analyzed to better assess each locality's true source characteristics. In this study, we adopt the highest X value from each sampling site, which is highlighted in bold font in Table 1. At any rate, duplicate and triplicate samples generally show good agreement between their helium isotope ratios with <1 R_A difference.

Helium concentrations from our samples are given in Table 1 and have been corrected for air contamination utilizing the following equation (Craig et al., 1978; Hilton, 1996):

$$\left[{}^4He \right]_C = \left[{}^4He \right]_M \times (X - 1)/X$$

The measured concentration values range between 0.284 x 10^{-6} (El Volcan) and 8.86 x 10^{-6} cm^3 STP/gH_2O (Ensenada) for fluid phase samples, significantly greater than air-equilibrated water (~4 x 10^{-8} cm^3 STP/gH_2O). Helium concentrations in the gas phase samples range between 170,000 x 10^{-6} and 0.986 x 10^{-6} cm^3 STP.

4.2 $\delta^{13}C$ (CO_2) Values

Gas and water phase samples were analyzed for their carbon isotope values ($\delta^{13}C$) and the results are reported in Table 1 in the per mil notation (‰). The measured values range between -19.39 to +9.08‰. Localities Santa Minerva (-10.83 and -19.39‰), PNA (-9.86, -12.60, -17.38‰), and San Borja (-12.46, -13.13, -17.62‰) show considerable variability in their duplicates. Water phase samples collected in 2014 have positive values with the exception of the Puertecitos sampling site. The highest value observed in this study is +9.08‰ found in the Ejido Uruapan site, which was re-sampled a year later and displayed a -4.47‰ signature. The lowest value of -19.39‰ is located in Santa Minerva. Heavier $\delta^{13}C$ signatures representative of MORB (-6.5‰; Sano and Marty, 1995) were found towards the eastern side of the Baja peninsula.

4.3 $CO_2/^3He$ Ratios

$CO_2/^3He$ ratios of the samples range between 0.000202 and 3257 ($x10^9$) and are given in Table 1. Samples collected in the El Volcan region exhibit the largest $CO_2/^3He$ ratios ($x10^{13}$), akin to crustal sources ($x10^{11}$ to 10^{13}; O'Nions and Oxburgh, 1988), whereas a majority of other sites exhibit MORB-like values (2×10^9; Marty and Jambon, 1987) with the only exception being Santa Minerva, which exhibits the lowest value of 0.000202 ($x10^9$).

4.4 Water Chemistry

The major ion water chemistry of the samples is reported in Table 3. The majority of groundwater samples collected from the 2014 and 2015 campaigns are classified as chloride waters with the exception of two samples identified as mixed $CaNaHCO_3$. Water samples for chemistry from Punta Estrella and Ensenada were not collected. Total dissolved solids (TDS) values range from 390 to 27729 ppm and alkalinity (as $CaCO_3$) values range between 45.1 and 2711.2 mg/kg of solution. Charge balance error calculations were conducted for our water samples utilizing the following equation (Hiscock, 2005):

$$CBE(\%) = \frac{(\sum cations - \sum anions)}{(\sum cations + \sum anions)} \times 100$$

An error of approximately ± 5% (Freeze and Cherry, 1979) is considered an acceptable value; however, charge balances calculated for some waters in this study are higher, in some instances, up to 9%. According to Fritz (1994), it becomes more difficult to achieve a good charge balance in dilute groundwater of very low TDS because errors become pronounced on samples with low concentration. For example, the groundwater sample from San Borja has the lowest TDS (390 mg/L) and the highest charge balance error (9.35%). On the other hand, waters with a TDS greater than 1000 mg/L tend to have large concentrations of few components and as a result the charge balance may not sufficiently evaluate the accuracy of minor components, thus also leading to large charge balance errors (Trick et al., 2008).

Saturation indices with respect to calcite are calculated using the USGS sponsored program PHREEQC (Parkhurst and Appelo, 2013). The saturation index is the state of

saturation of a mineral in an aqueous solution. By calculating the saturation indices, it is possible to determine the equilibrium state of groundwater with respect to a given mineral: in this case, calcite (Hiscock 2005). Saturation indices for the samples range between -0.87 and +1.34, with 4 having positive values and the majority (8) exhibiting negative values. Positive values indicate oversaturation with respect to calcite, which would be expected to result in its precipitation. A negative value indicates undersaturation with respect to calcite and thus dissolution of calcite is expected (Hiscock, 2005).

A trilinear, or Piper, diagram is a useful way of visualizing the results of a large number of samples in a single plot (Piper, 1944). The percentage of total meq/L of cations is plotted on the left ternary, using Ca^{2+}, Mg^{2+} and (Na^{+} + K^{+}) as the three axes of the triangle. Similarly, anions are plotted in the right ternary using the percent meq/L of Cl^{-}, SO_4^{2-}, and (CO_3^{2-} + HCO_3^{-}) as the three axes. The diamond between the two triangles shows projections from the anion triangle and the cation triangle to a field that shows the overall major ion water chemistry. Based on where the data points lie in the center diamond, the classification of water types or hydrochemical facies can be determined.

Table 3: Water Chemistry from Baja California 2014 and 2015

Location	Latitude	Longitude	T (°C)	pH	Water Type	TDS (ppm)	Alkalinity[a] (mg/kg)	Cl (mg/L)	SO_4 (mg/L)	Na (mg/L)	K (mg/L)	Ca (mg/L)	Mg (mg/L)	Charge Balance (%)	S.I.[b]
Cascada Arroyo Guadalupe	N 32°03′42″	W 116°15′54″	52	8.5	NaCl	643.5	55.27	278	56	204	3	<1	3	3.44	-0.87
Santa Minerva	N 31°59′58″	W 116°05′39″	58.3	9.26	NaCl	344.5	136.64	56	45	97	1.8	1.3	<1	3.74	0.21
Rancho Agua Caliente	N 31°49′52″	W 116°23′17″	43.2	9.29	NaCl	481	83.26	138	63	136	2	<1	1.7	3.21	-0.17
Rancho San Carlos	N 31°47′43″	W 116°26′05″	41.3	9.22	NaCl	526.5	90.25	129	97	147	3.7	<1	1.2	3.6	-0.23
La Jolla - Villarino	N 31°43′09″	W 116°39′43″	63.6	8	NaCl	14885	125.92	6343	413	3084	148	593	166	2.21	1.34
Ejido Uruapan	N 31°37′58″	W 116°26′05″	55.3	9.21	NaCl	773.5	71.83	232	107	204	3.5	1.2	2.9	3.54	-0.18
Ejido Uruapan (re-sample)	N 31°37′58″	W 116°26′04″	57.7	9	NaCl	877.5	76.05	235	109	211	3.5	<1	2	3.34	-0.34
Las Positas	N 31°23′18″	W 115°47′01″	38.2	8.5	NaCl	598	136.56	139	65	153	1.4	<1	<1	4.78	-0.63
Punta Estrella	N 30°56′40″	W 114°44′01″	31.1	5.91	n.d.	27729	n.d.	n.d.	n.d.	n.d.	n.d.	n.d.	n.d.	n.d.	n.d.
Plan Nacional Agrario	N 30°38′51″	W 115°12′27″	64.1	9	NaCl	1014	45.12	123	349	243	7	<1	3.9	1.53	-0.63
Puertecitos	N 30°20′46″	W 114°38′10″	61.2	6.66	NaCl	27495	292.69	14400	1420	7629	361	2925	157	6.37	0.99
El Volcan-2	N 29°59′33″	W 114°46′15″	23.4	6.5	Mixed $CaNaHCO_3$	2892.5	2711.18	626	<2	767	49	403	3.7	6.07	0.78
San Borja	N 28°44′25″	W 113°45′07″	35.7	9	Mixed $CaNaHCO_3$	390	167.52	77	25	100	0.99	<1	<1	9.35	-0.13

Temperature, pH, and TDS measurements were conducted in the field.
Ensenada 2001 water chemistry not available.
[a] Alkalinity reported as $CaCO_3$.
[b] Saturation index as calcite.
n.d. = not determined.

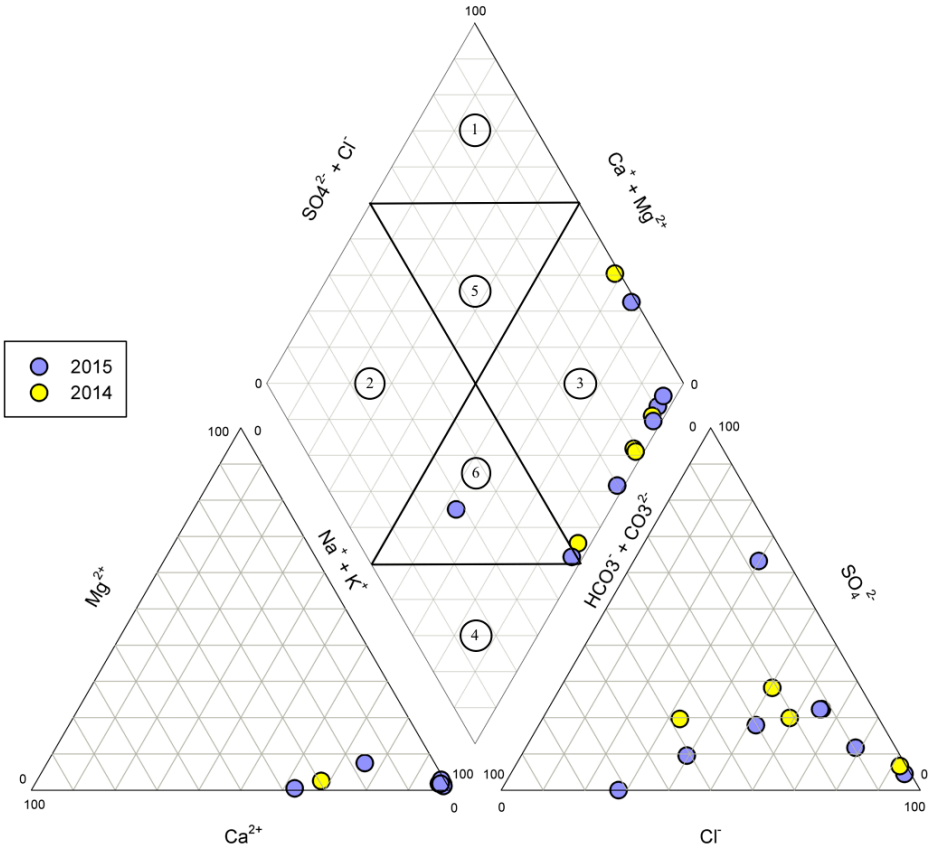

Figure 4: Piper plot of groundwaters from northern Baja California. Numbered regions represent the classification of waters. 1) $CaCl_2$, 2) $CaHCO_3$, 3) NaCl, 4) $NaHCO_3$, 5) Mixed CaMgCl, 6) Mixed $CaNaHCO_3$.

5. DISCUSSION

In the following sections, we discuss the distribution and provenance of helium and carbon collected from hot springs throughout northern Baja California. we interpret data the identify primary source characteristics and any potential secondary modification. In order to better understand the mantle structure of this region, the geochemical data will be compared to other geophysical work for a broader perspective.

5.1 Spatial Variations in Helium Isotope Ratios ($^3He/^4He$)

The helium isotope ratios identified in northern Baja California region are consistent with previous studies conducted within the area (Vidal et al., 1982; Forrest et al., 2005). All samples exhibit $^3He/^4He$ a lot higher than the 0.02-0.05 R_A crustal helium value (Andrews, 1985), signifying a higher mantle helium contribution. As discussed below, a number of parameters such as proximity to faults, the structural geology of sampling sites, and the distance to volcanic centers may affect controls on helium isotope ratios.

5.1.1 Fault Proximity

Previous work conducted in the central and southern portion of the San Andreas Fault (Kennedy et al., 1997; Kulongoski et al., 2005; 2013) has revealed significant mantle helium contributions, ranging from 1 to 50% of the total helium. More importantly, a modest trend is observed between the helium isotopic composition of samples and the distance from the strike of the fault. Higher $^3He/^4He$ (~0.5 to 2.1 R_A)

were recorded within a 20 km distance from the San Andreas Fault, whereas lower $^{3}He/^{4}He$ (~0.2 to 1.0 R_A) were observed at distal localities of 20-80 km from the fault (Kennedy et al., 1997; Kulongoski et al., 2013).

Table 4: Relationship between helium isotopes and distance to a fault

Sample Location	**Distance to Fault**	**R_C/R_A**
La Jolla-Villarino	0.05 km (Agua Blanca)	0.22
Cascada Arroyo Guadalupe	0.8 km (Vallesitos fault)	0.40
Las Positas	1.0 km (Agua Blanca)	0.55
Rancho Agua Caliente	2.3 km (Tres Hermanos)	0.33
Ejido Uruapan	3.3 km (Agua Blanca)	0.65
Ejido Uruapan (re-sample)	3.3 km (Agua Blanca)	0.55
Santa Minerva	3.7 km (Vallesitos faut)	0.11
Plan Nacional Agrario	5.2 km (San Pedro Mártir)	0.30
Rancho San Carlos	8.0 km (Tres Hermanos)	0.24
Punta Estrella	33 km (MOR)	1.13
San Borja	47 km (MOR)	0.37
Puertecitos	61 km (MOR)	1.74
El Volcan	72 km (MOR)	1.31

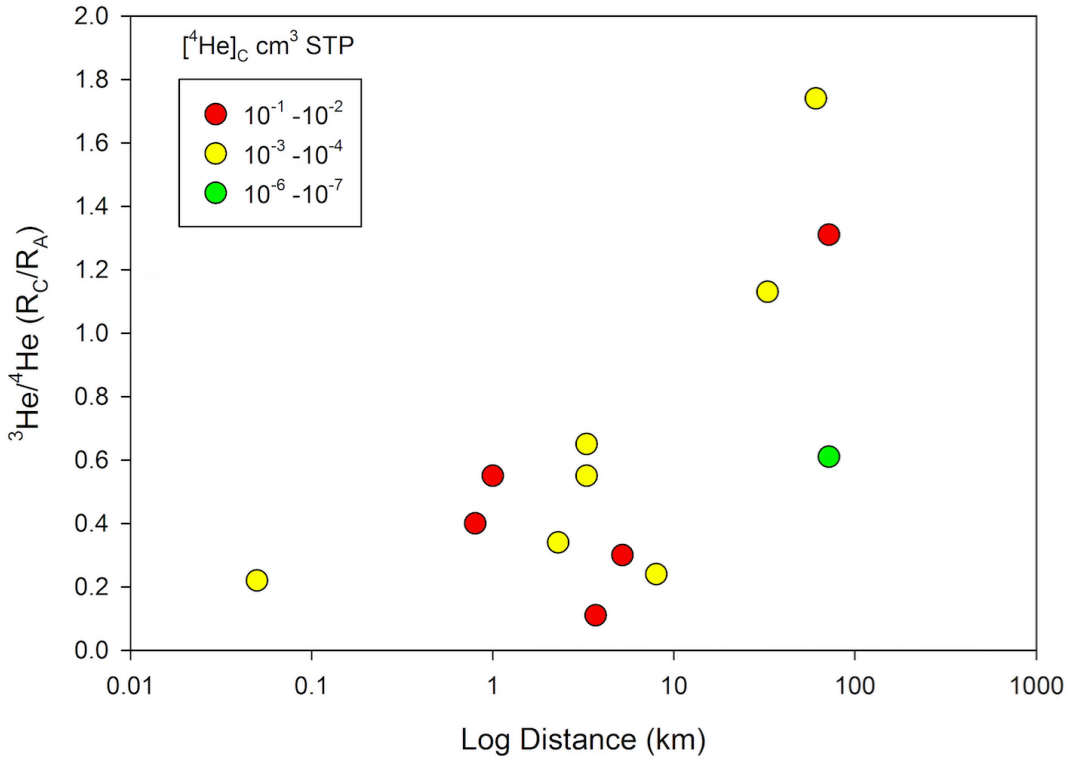

Figure 5: Helium isotopes (R_C/R_A) of samples collected in Baja California plotted as a function of distance (km) to the nearest fault.

Helium isotope ratios significantly higher (> 0.1 R_A) than crustal values may result from the transport of helium and other fluids from the upper mantle through faults that reach the shallow crust (Ballentine et al., 2002). However, radiogenic helium produced by the decay of uranium and thorium in the crust effectively dilutes mantle helium to produce the helium ratios observed at the surface. In order to further elucidate this effect on our samples, a plot of $^3He/^4He$ versus distance to the nearest fault (with color representing helium concentration) is shown in Figure 5. The sample locations, respective $^3He/^4He$, and the distance between the sampling sites and the nearest fault are given in Table 4. Surprisingly, our samples demonstrate the opposite effect from that observed in the San Andreas Fault. The $^3He/^4He$ (0.11 to 0.65 R_A) of samples located

closest to a fault (~10 km distance) are lower when compared to the $^{3}He/^{4}He$ (0.53 to 1.74 R_A) of samples located farther away from a fault (> 30 km). This indicates that although strike-slip faulting in the west plays a role in facilitating volatiles to the surface, other controls may be responsible for the eastern localities' elevated $^{3}He/^{4}He$ values.

5.1.2 Structural Provinces

A second possible influence on helium isotopes may be the structural geology of sampling sites. The main continental regions where mantle helium is found include areas undergoing extension, subduction-type volcanoes, major fault systems as well as kimberlite pipes and other xenolith-bearing localities (Hilton and Porcelli, 2003). In Baja, $^{3}He/^{4}He$ >1 R_A have also been associated with regions of active extension as a result of crustal thinning (Forrest et al., 2005; Kulongoski et al., 2005). Thus, we examine the relationship between the $^{3}He/^{4}He$ of our samples and the four main structural provinces within the peninsula and the Gulf of California: the Gulf Extensional Province (GEP) along eastern Baja, the relatively unextended central and western portion of the peninsula, the transpeninsular strike-slip province north of the Agua Blanca fault, and the sheared continental borderland (Gastil et al., 1975). Two of our sample localities lie within the boundary of the GEP, three are in the central portion of the peninsula, the majority (7) of our samples are in the transpeninsular strike-slip province, but no sample from the offshore continental borderlands (Figure 6). Punta Estrella and Puertecitos exhibit some of the highest $^{3}He/^{4}He$ ratios (1.13 and 1.74 R_A) and are located near the east coast within the GEP boundary. To the west, the Main Gulf Escarpment serves as a boundary between the stable central region and the GEP. The escarpment is formed by a

series of concave normal faults (primarily the north-south striking San Perdo Martír fault) that dip to the east, terminating near Puertecitos. The province is underlain by Cretaceous granodiorite and tonalite of the Peninsular Range batholith that intruded Paleozoic and Mesozoic arc and continental margin rocks (Gastil et al., 1975).

The central portion of the peninsula has been the most stable area of Baja California, with major faults uncommon throughout this region. This structural province extends from the Agua Blanca fault to the north to the Rosarito fault to the south and the Main Gulf Escarpment to the east (Gastil et al., 1975). The sampling locations of PNA, El Volcan, and San Borja are located within this area of the peninsula along the western edge of the Main Gulf Escarpment. The $^{3}He/^{4}He$ of PNA and San Borja are low (0.30 and 0.37 R_A) with El Volcan being the highest (1.31 R_A). PNA is located within the Sierra San Perdo Martír, a batholithic terrain with thick continental crust. To the south, near San Borja, the area is dominated by a large high-magnesian andesite volcanic field. Here, the Cretaceous igneous and metamorphic basement is overlain by Tertiary sedimentary rocks and Miocene calc-alkaline lavas from the Comondú arc (Pallares et al., 2008; Negrete-Aranda et al., 2010).

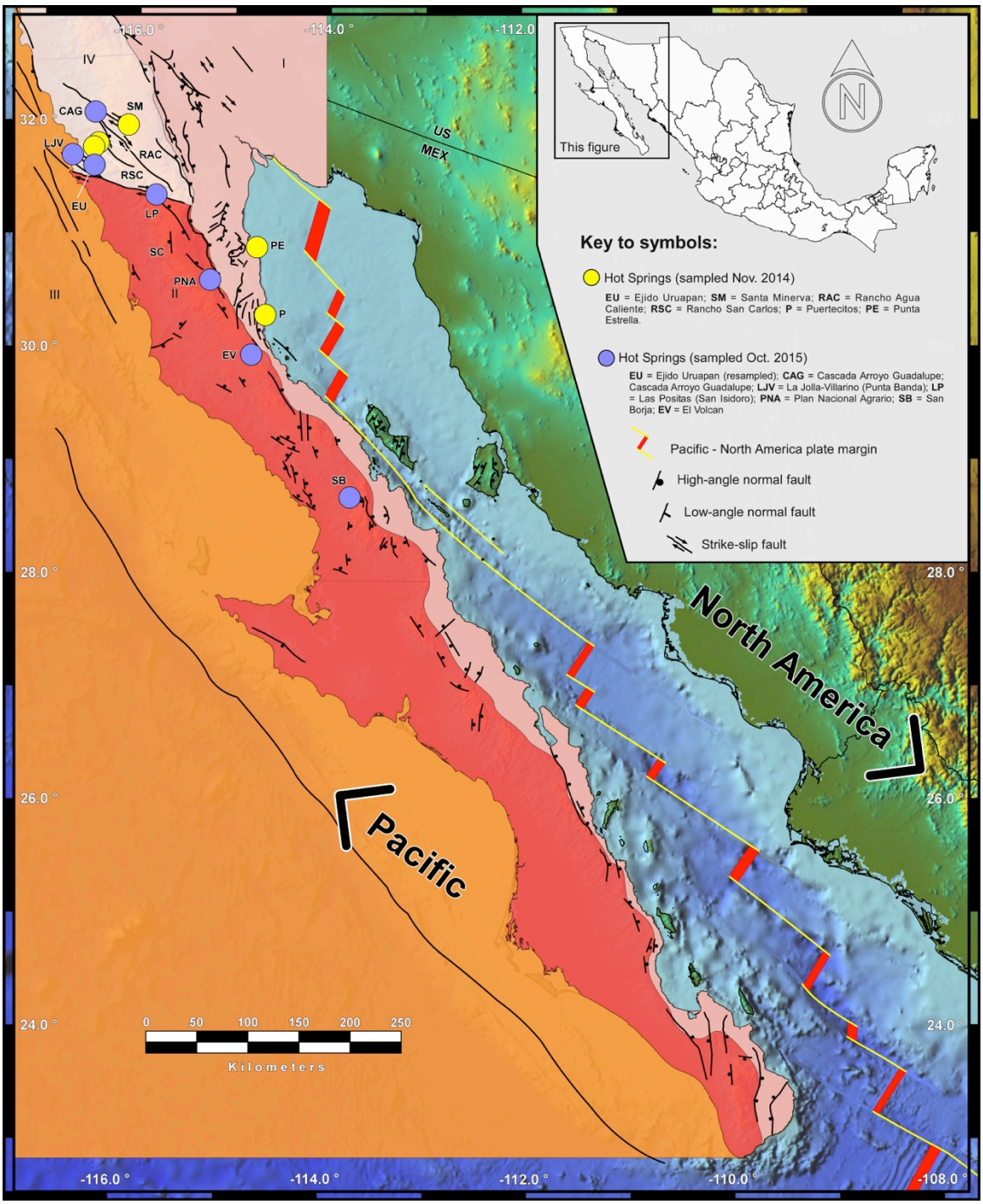

Figure 6: Four major structural provinces of Baja California: I) Gulf Extensional Province along eastern Baja (pink), II) unextended central and western Baja (red), III) sheared continental borderland (orange), IV) transpeninsular strike-slip province (tan). Figure modified from Spelz et al., 2017.

The transpeninsular strike-slip province contains major strike-slip fault systems that transect the peninsula in northern Baja California. The majority of our samples (7) lie in this region and exhibit $^{3}He/^{4}He$ ratios with a significant (1 to 8%) mantle component. The Agua Blanca Fault is associated with La Jolla-Villarino, Ejido Uruapan, and Las Positas hot springs, the Vallecitos Fault is associated with the Cascada Arroyo Guadalupe and Santa Minerva hot springs, and the Tres Hermanos Fault is associated with Rancho Agua Caliente and Rancho San Carlos hot springs. The largest structural element in this region is the Agua Blanca Fault, which extends 140 km from the San Matias pass in the east, to Ensenada Bay in the west, and continues offshore. This fault has a transitional strike-slip to normal fault behavior, which forms a half-graben that characterizes the Todos Santos Plain and Punta Banda Peninsula (Gastil et al., 1975). In terms of geology, three main rock groups, pre-batholitic, batholitic and post-batholitic, constitute the main lithologic assemblages in this region. The pre-batholitic group is made up of volcaniclastic Alisitos Formation of the Lower Cretaceous, which consists of an arc assemblage of andesitic flows and volcaniclastic deposits (Perez-Flores et al., 2004). The rugged ranges that extend towards the east are the batholitic group composed of crystalline plutonic rocks of the tonalite, gabbro and granodiorite type (Perez-Flores et al., 2004). The post-batholitic group is made up of the Upper Cretaceous marine sedimentary Rosario Formation, Miocene basalt, andesites, and Quaternary alluvium and beach deposits (Arango-Galvan et al., 2011).

5.1.3 Volcanic Proximity

Another possibility that may influence helium isotopes is the distance of sampling locality to a nearest volcanic center. Previous studies (Sano et al., 1984; Marty et al., 1989; Barry et al., 2013) have shown that the highest $^{3}He/^{4}He$ ratios are found closest to volcanic edifices and $^{3}He/^{4}He$ ratios decrease with increasing distance from the volcanic center. However, all but three sampling sites from our study are in excess of 100 km to the nearest volcanic center. The Puertecitos (1.74 R_A) and San Borja (0.53 R_A) sampling localities are in close proximity to ancient volcanic fields that do not exhibit, present day activity. The Puertecitos Volcanic Province is composed of Tertiary volcanic sequences, the youngest being Pliocence ignimbrites (~3 Ma; Martín-Barajas et al., 1995) and the San Borja Volcanic Field is comprised of hundreds of scoria cones with the latest volcanic activity occurring around 3.5 Ma (Negrete-Aranda et al., 2010). Lastly, El Volcan (1.31 R_A) is approximately 30 km to the nearest volcanic center of San Luis Island, a volcanic island located offshore that last erupted in the Quaternary. Despite this, it is unlikely this has an effect on helium isotopes due to the volcano's small 4.5 km^2 area and elevation of 180 meters (Paz Moreno and Demant, 1999).

5.1.4 Helium Isotopic Characteristics of Northern Baja California

We conclude that variations in the observed $^{3}He/^{4}He$ are multi-faceted and complex. The modest mantle contribution in the $^{3}He/^{4}He$ from the majority of our samples can be attributed to the proximity (<10 km) to active faults that lie in the tectonically active transpeninsular strike-slip province. This setting suggests that these faults act as conduits,

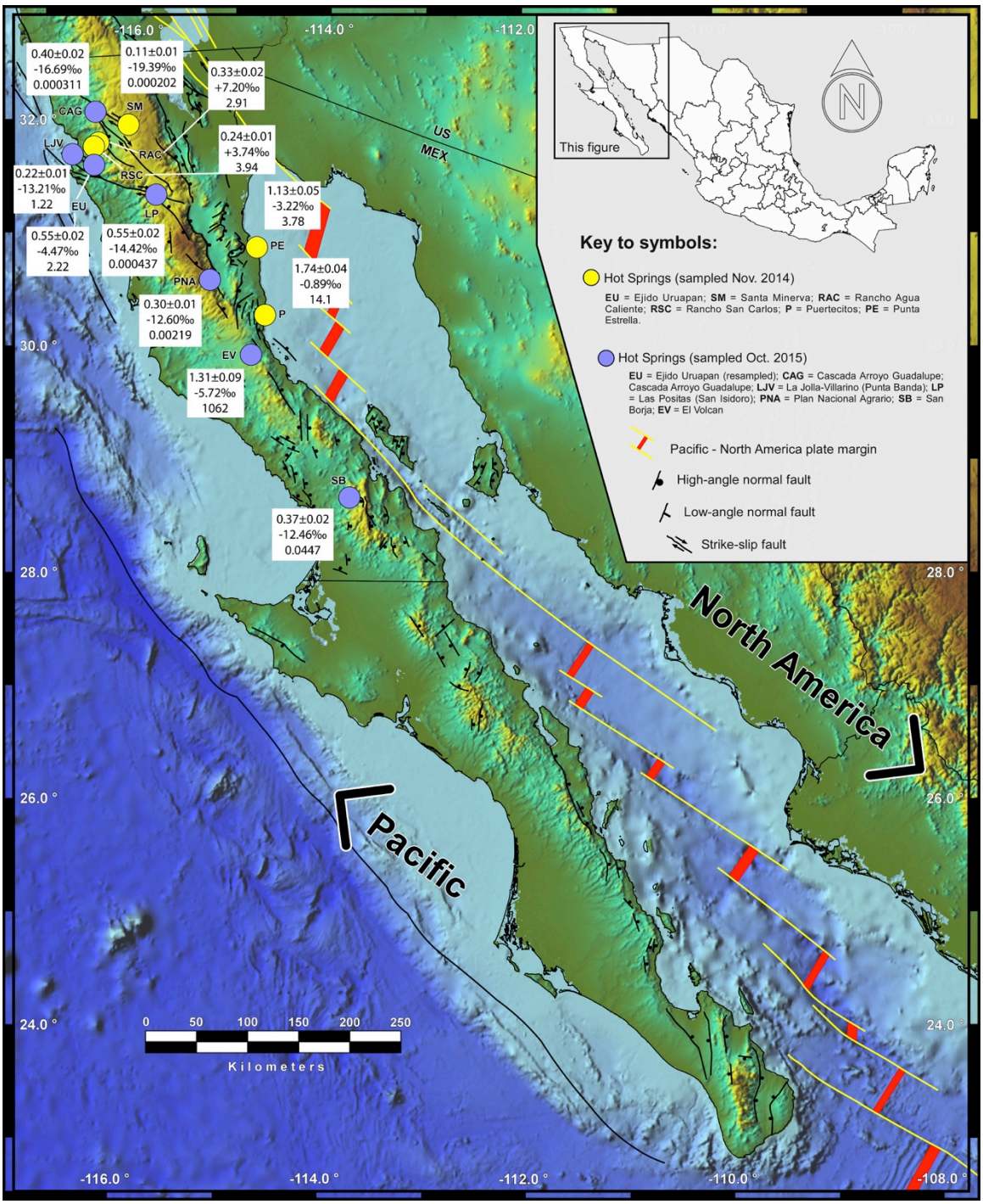

Figure 7: Map of the study area illustrating sample localities with corrected helium isotopes (R_C/R_A), carbon isotopes $\delta^{13}C$ (CO_2) VPDB, and $CO_2/^3He$ values (10^9). Figure modified from Spelz et al., 2017.

allowing meteoric water to be heated by the higher than average heat flow, and produce numerous geothermal areas that facilitate the release of mantle helium (Gullec et al., 2002). However, the localities that display the highest $^{3}He/^{4}He$ in this study are located in the east, within the GEP and the stable region of the peninsula, with the exception of the PNA (0.30 R_A) and San Borja (0.37 R_A) localities. To visualize the $^{3}He/^{4}He$ aerial distribution, Figure 7 presents adopted values (R_C/R_A, $\delta^{13}C_{CO2}$, and $CO_2/^{3}He$) for each locality in order to gain a west-east perspective. With respect to helium, modest $^{3}He/^{4}He$ ratios lie in the west, followed by a slight decrease in the middle of the peninsula, and an increase in the east. The crustal thickness of the Peninsular Ranges and the GEP may play an important role in this scenario. According to teleseismic studies, the depth to the Moho beneath northern Baja California varies 33 km near the Pacific coast, thickens gradually toward the east to 40 km beneath the western Peninsular Ranges, and then abruptly thins to 15-18 km beneath the center and margins of the Gulf of California (Lewis et al., 2001). Furthermore, the region of extension may permeate the lower crust of the eastern Peninsular Ranges, tens of kilometers west of the zone of extensional deformation observed at the surface (Lewis et al., 2001). Thus, lower helium isotopes values observed at PNA may be the result of fluids traversing thicker crust, increasing the potential of radiogenic helium addition, while still displaying a mantle contribution of 3.5%. The high $^{3}He/^{4}He$ values in Punta Estrella, Puertecitos, and El Volcan reflect extensional deformation of the lower crust in response to adjacent rifting of the GEP. In addition, the distance of a sampling locality to a continental volcanic center does not exhibit a notable influence due to the lack of recent volcanic activity and vast distance (>100 km in some instances) between sampling sites and the nearest volcanoes.

5.2 Observed CO_2 – ^3He – ^4He Characteristics

In order to evaluate whether the water and gas samples taken from northern Baja California are representative of MORB-like or arc-like volatiles with or without a strong (superimposed) crustal input, we use a CO_2-^{3}He-^{4}He ternary plot (Giggenbach et al., 1993). This type of plot has been used in previous studies, e.g., the East African Rift in Tanzania (Barry et al., 2013) and the North Anatolian Fault in Turkey (De Leeuw et al., 2010) to identify and assess controls on the He-CO_2 features of gas and water samples.

Samples from this study are plotted in Figure 8 with MORB ($CO_2/^3He = 2 \times 10^9$, 8 R_A), crustal ($CO_2/^3He = 5\text{-}50 \times 10^{12}$, 0.02 R_A) and air ($CO_2/^3He = 5.47 \times 10^7$, 1 R_A) end-members (O'Nions and Oxburgh, 1988). The majority of the samples lie towards the right of the ternary diagram pointing to contributions from radiogenic (crustal) helium, and plot below the narrow MORB $CO_2/^3He$ ratio of 2×10^9. The three samples (Punta Estrella, Puertecitos, and El Volcan) with the highest $^3He/^4He$ ratios plot on a trajectory towards the CO_2 apex (high $CO_2/^3He$), suggesting mixing between crustal and mantle end-members. Similar trends have been found in the Rungwe Volcanic Province (Barry et al., 2013), where samples plotting at the apex have unusually high $CO_2/^3He$ ratios and are usually representative of samples that have experienced hydrothermal phase separation, due to the fact that CO_2 is more soluble in water than He. Samples plotting at the base of the diagram, those with very low $CO_2/^3He$ values, are thought to have experienced CO_2 loss by processes such as calcite precipitation. These shallow level processes act to modify source signatures of $CO_2/^3He$ (and $\delta^{13}C$) during transport to the surface (Barry et al., 2013). In the following discussion, we assess whether the variations

of CO_2-^{3}He-^{4}He of the samples reflect binary mixing between different end-member components or if other processes are involved.

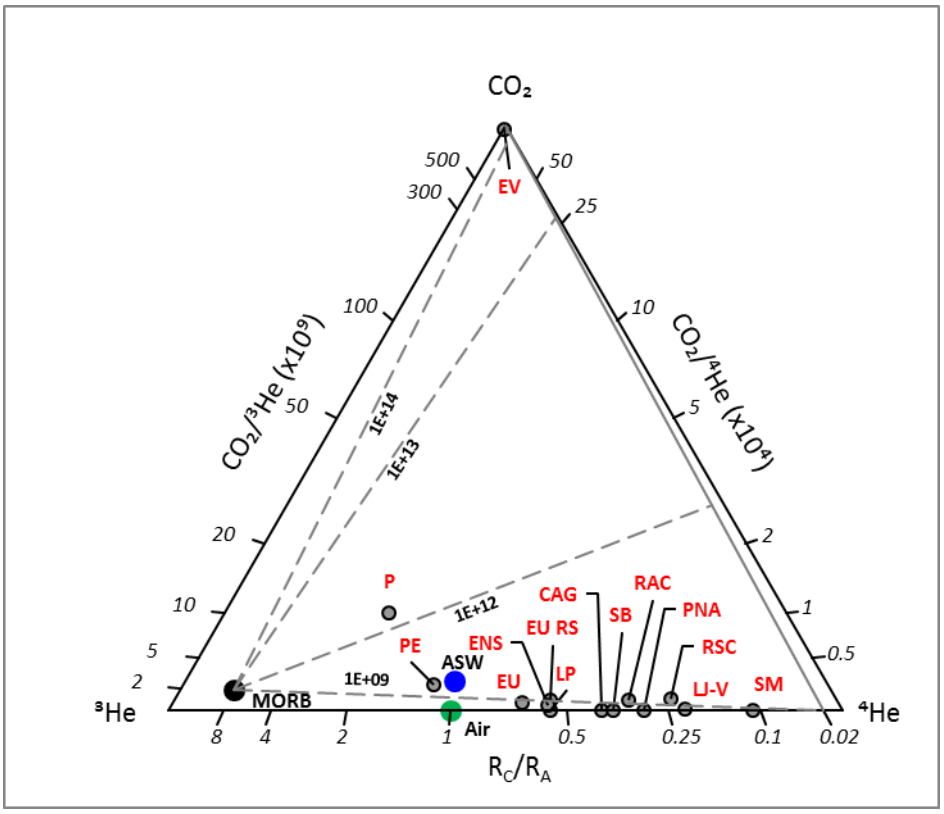

Figure 8: Ternary plot of CO_2, ^{3}He, and ^{4}He for gas and water samples from northern Baja California. For reference, we plot MORB (8 ± 1 R_A) with a black circle and Air (1 R_A) with a green circle.

5.2.1 Controls on He – CO_2 Systematics I: Sampling Gas vs. Water

Phase separation within a hydrothermal system can significantly alter $CO_2/^3He$ and $\delta^{13}C$ values due to solubility differences between CO_2 and He in water (Ellis and Golding, 1963). In this situation, where CO_2 has a higher solubility in aqueous fluids than He (Ozima and Podosek, 1983), He will preferentially partition into the vapor phase relative to CO_2 leaving the residual water phase with a higher $CO_2/^3He$ relative to starting values. Phase separation can also have an effect on the $\delta^{13}C$ as fractionation occurs between $^{13}CO_2$ and $^{12}CO_2$ during partitioning of CO_2 between water vapor and liquid (Vogel, 1970).

Since six of our localities display low (10^5-10^8) $CO_2/^3He$ values, there is an indication that hydrothermal phase separation may play a role in modifying some samples. These localities (Cascada Arroyo Guadalupe, Santa Minerva, Las Positas, PNA, San Borja, and Ensenada) exhibit low $CO_2/^3He$ ratios ranging between 10^5 and 10^8 and low $\delta^{13}C$ values ranging between -9.86 to -19.39‰. In an ideal scenario, both gas and water samples would be collected for each locality to allow a comprehensive comparison between the two phases. Unfortunately, not all sampling sites allowed for both water and gas sampling with the exception of San Borja, El Volcan, and Ejido Uruapan. In this case, there is little difference in the $CO_2/^3He$ ratios between the San Borja water phase sample (BAJA-32) and its corresponding gas phase sample (BAJA-34, see Table 1). Therefore, it is not clear whether hydrothermal phase separation alone can explain the $CO_2/^3He$ characteristics of this particular locality. However, $\delta^{13}C$ fractionation is apparent in the water and gas values at El Volcan (-5.72 and -9.05‰, respectively) and

San Borja (-12.46 and -17.62‰, respectively), consistent with the ~4‰ difference that Vogel predicted (see Figure 9).

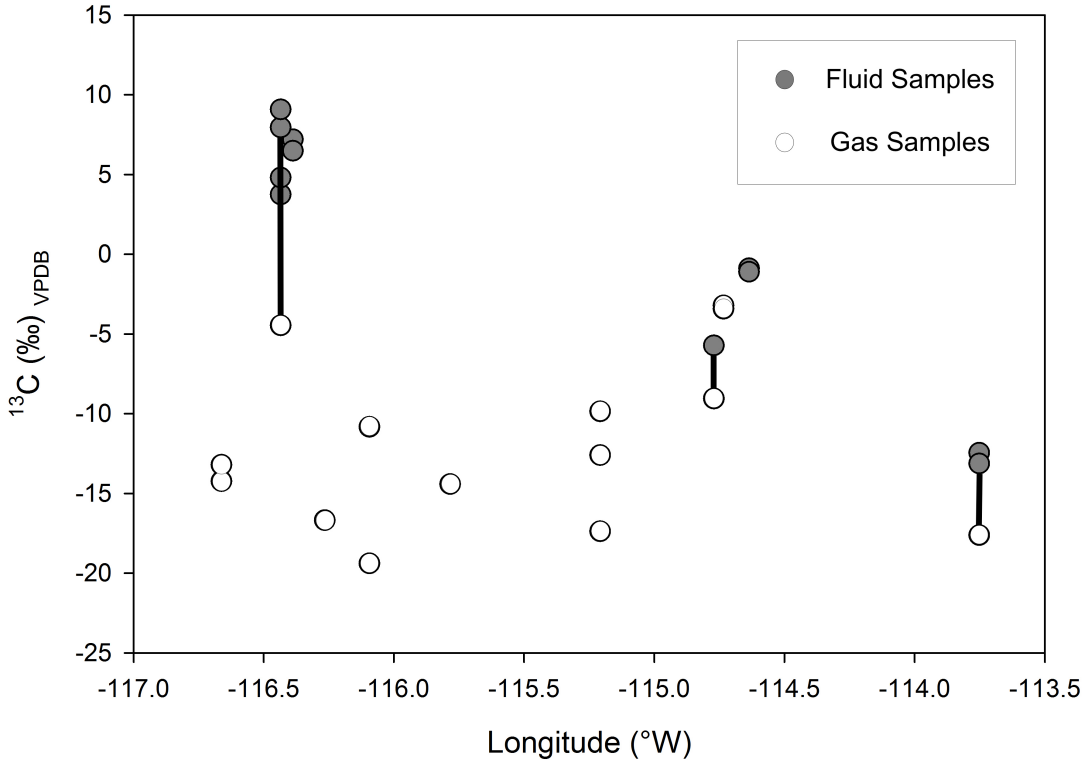

Figure 9: $\delta^{13}C$ plotted versus longitude for gas and fluid samples from northern Baja California. Vertical tie-lines connect gas and fluid phase samples form the same locality.

5.2.2 Controls on He – CO_2 Systematics II: Calcite Precipitation

A process that can act to lower the $CO_2/^3He$ ratios and fractionate $\delta^{13}C$ is the loss of CO_2 through calcite precipitation (Ray et al., 2009). Interaction with country rock during the cooling and/or mixing of fluids deep within the hydrothermal system tends to leave fluids abundant in Na^+, Ca^{2+}, Mg^{2+}, and HCO^{3-}/CO_3^{2-} ions (Spane and Webber, 1995; McLing et al., 2001). The CO_2 rich fluids and gases react with these ions to precipitate carbonate minerals. During this reaction, CO_2 remains in the form of calcite,

leading to lower $CO_2/^3He$ ratios and more positive $\delta^{13}C$ in residual fluids. This would result in samples plotting on the base of the CO_2-^3He-^4He diagram.

5.3 $CO_2/^3He$ – $\delta^{13}C$ Mixing Model

Figure 10 is a plot of a three-component mixing model, frequently used to resolve MORB, marine limestone, or organic sediment derived carbon contributions using $CO_2/^3He$ and $\delta^{13}C$ data (Sano and Marty, 1995; Kulongoski et al., 2013). Thus, we plot the $CO_2/^3He$ ratios as a function of $\delta^{13}C$ for water samples with three end-members: Limestone (L), Mantle (M), and Sediment (S) in Figure 10. The assumed end-member composition for both $\delta^{13}C$ and $CO_2/^3He$ compositions are $\delta^{13}C$ = -6.5‰, $CO_2/^3He$ = $2x10^9$ for (M), $\delta^{13}C$ = 0‰, $CO_2/^3He$ = 10^{13} for (L) and $\delta^{13}C$ = -30‰, $CO_2/^3He$ = 10^{13} for (S) (Sano and Marty, 1995). In addition, binary mixing trajectories and fractions between end-members are illustrated on the plot.

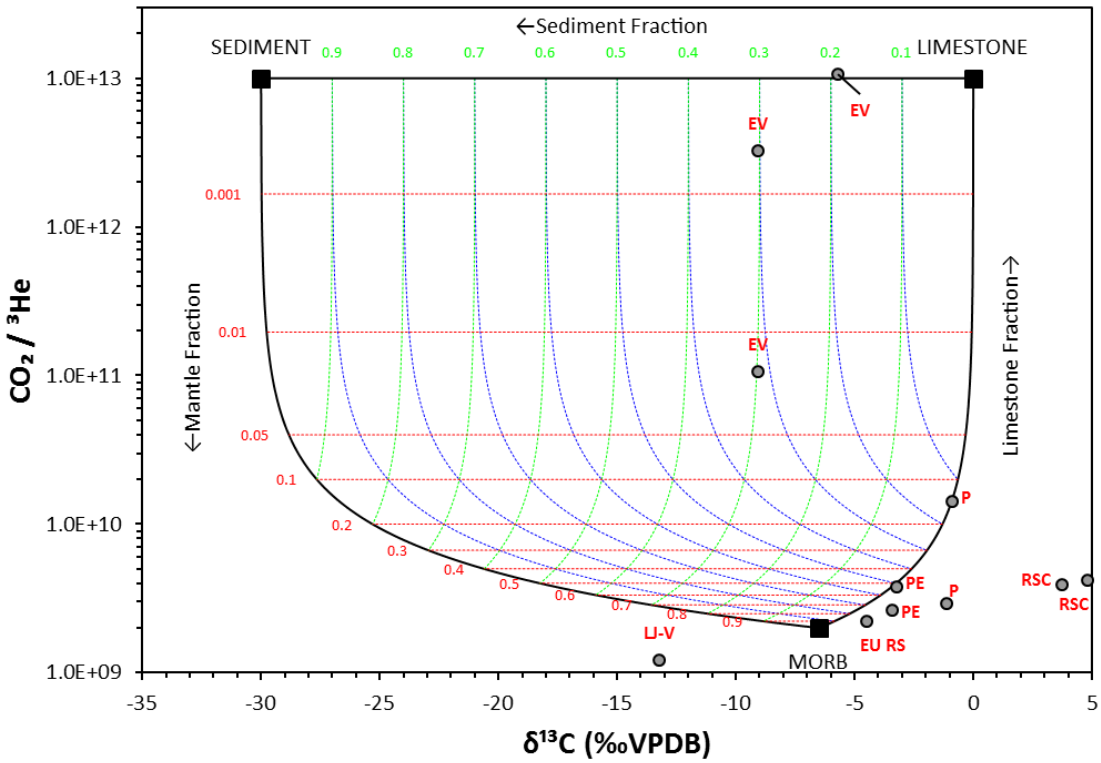

Figure 10: Plot of $CO_2/^3He$ versus $\delta^{13}C$ for northern Baja California fluid samples. Mantle (M) values: $\delta^{13}C$=-6.5‰, $CO_2/^3He=2x10^9$. Limestone (L) values: $\delta^{13}C$=0‰, $CO_2/^3He=10^{13}$. Sediment (S) values: $\delta^{13}C$=-30‰, $CO_2/^3He=10^{13}$. Note that Cascada Arroyo Guadalupe, Santa Minerva, Ejido Uruapan, Las Positas, Plan Nacional Agrario, San Borja, and Ensenada are not shown.

As seen in Figure 10, the majority of our samples (except El Volcan and Puertecitos) plot outside the theoretical mixing lines and are therefore unrepresentative of mixing. Typically, the L-M-S model works well in high temperature volcanic systems coupled with samples that undergo little to no modification. While the Puertecitos and El Volcan samples may be explained by L-M-S end-member mixing, the remaining samples have been modified due to phase separation and calcite precipitation. Using a simple calcite precipitation model (see Figure 11), we observe that Rancho Agua Caliente, Rancho San Carlos, Ejido Uruapan, Puertecitos, El Volcan, and Ensenada fluid phase samples that plot outside the L-M-S mixing lines can be explained by CO_2 loss.

Assuming a crustal starting composition of $CO_2/^3He = 2x10^{11}$ and $\delta^{13}C = -4‰$, as carbon is subsequently removed by calcite precipitation, we observe highly fractionated carbon isotopes with atypical and positive $\delta^{13}C$ signatures.

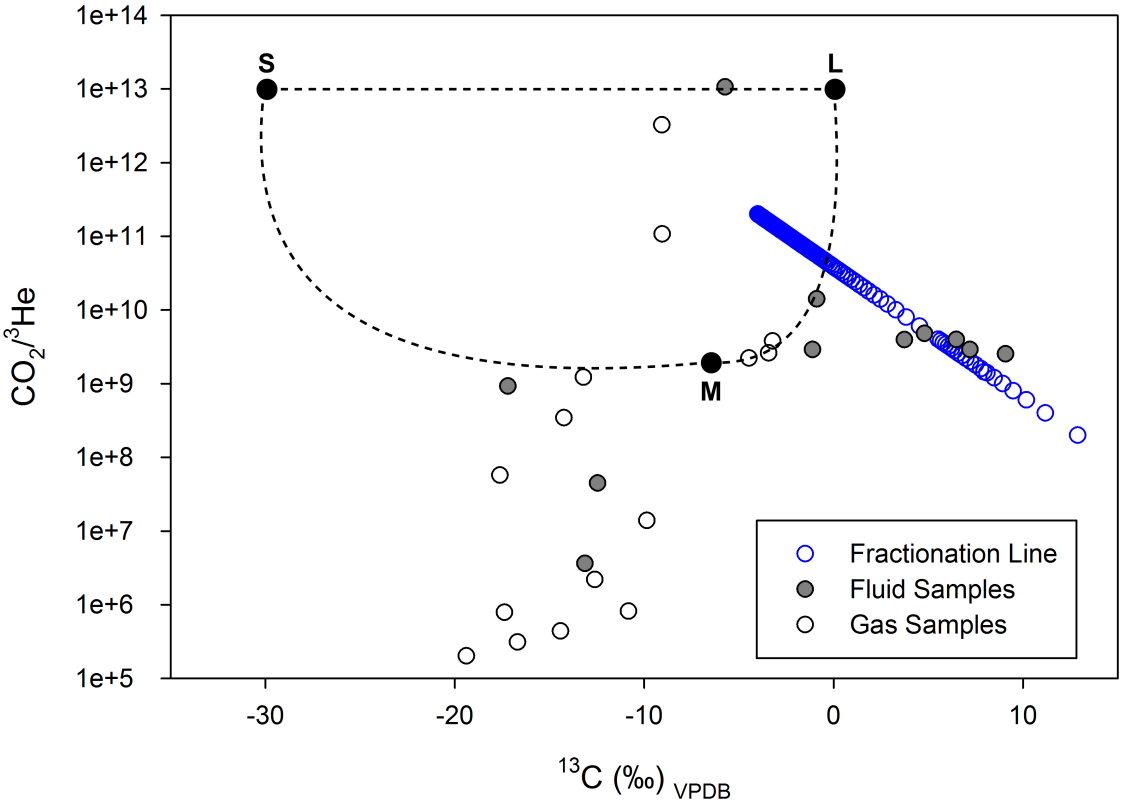

Figure 11: Plot of $CO_2/^3He$ versus $\delta^{13}C$ for northern Baja California fluid samples. Mantle (M) values: $\delta^{13}C$=-6.5‰, $CO_2/^3He=2x10^9$. Limestone (L) values: $\delta^{13}C$=0‰, $CO_2/^3He=10^{13}$. Sediment (S) values: $\delta^{13}C$=-30‰, $CO_2/^3He=10^{13}$. Starting composition assumed to be $CO_2/^3He = 2x10^{11}$ and $\delta^{13}C = -4‰$.

In order to quantify the relative proportions of CO_2 derived from each respective end-member component, the mass fractions of three major sources of carbon are quantitatively calculated using the following equations (Sano and Marty, 1995):

$$(^{13}C/^{12}C)_O = f_M(^{13}C/^{12}C)_M + f_L(^{13}C/^{12}C)_L + f_S(^{13}C/^{12}C)_S$$

$$1/(^{12}C/^3He)_O = f_M/(^{12}C/^3He)_M + f_L/(^{12}C/^3He)_L + f_S/(^{12}C/^3He)_S$$

$$f_M + f_L + f_S = 1$$

Table 5: Carbon Provenance

Sample Location	Mantle %	Limestone %	Sediment %
Puertecitos	14.2	85.8	0.0
El Volcan	0.0	80.9	19.1

where subscripts M, L, and S correspond to end-members Mantle, Limestone, and Sediment with end-member compositions as mentioned above. Calculated results are given in Table 5. Of the samples that fall within the L-M-S model, El Volcan has CO_2 contribution primarily from limestone (81%) and sediment (19%) and Puertecitos has a similar limestone input (86%) coupled with a minor mantle contribution (14%).

5.4 He – CO_2 Crustal-Mantle End-member Contributions

Figure 12 illustrates a R/R_A – $CO_2/^3He$ plot containing a series of curves representing binary mixture of mantle-derived gas and crustal-derived gases of various $CO_2/^3He$ values on logarithmic scales. It can be used to evaluate correlations between mantle-derived and crustal gases (O'nions and Oxburgh, 1988). Volatiles released from MORB result in nearly constant $CO_2/^3He$ values (~2 x 10^9; Marty and Jambon, 1987), whereas crustal rocks are characterized by several orders of magnitude higher (10^{11}-10^{13}) (O'Nions and Oxburgh, 1988) $CO_2/^3He$ values. In Figure 12, the observed $CO_2/^3He$ varies from 10^5-10^{13}. Significantly, half of the samples plot close to the mantle value but are characterized by much lower $^3He/^4He$ (0.22 - 0.65 R_A) than a typical mantle signature (8 R_A). Low $^3He/^4He$ and low, mantle-like $CO_2/^3He$ ratios suggest that the crustal component has low $CO_2/^3He$ ratios or the $CO_2/^3He$ ratio has been modified (De Leeuw et al., 2010). Across all samples, $^3He/^4He$ ratios are generally constant within one order of

magnitude, but lie on different mixing trajectories, suggesting the trends cannot be explained by simple binary mixing.

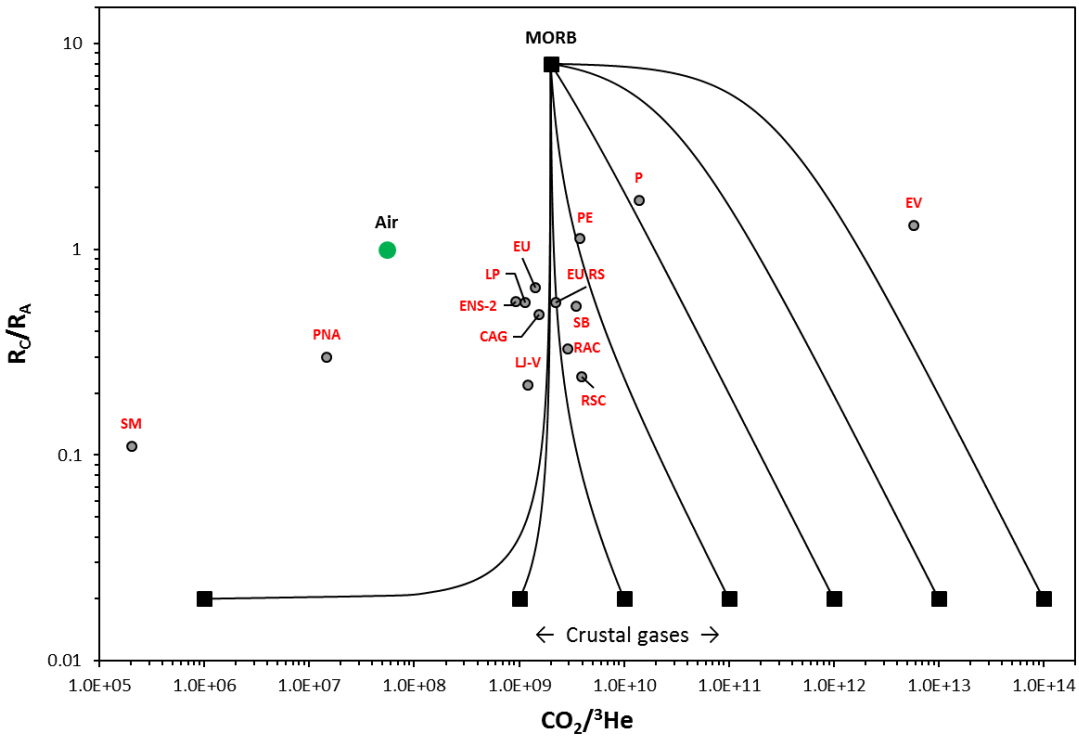

Figure 12: $CO_2/^3He$ versus He-isotopes with mixing trajectories between MORB and various crustal $CO_2/^3He$ end-members (1 x 10^7 – 1 x10^{14}).

5.5 Mantle Velocity Anomalies and Helium Isotope Ratios ($^3He/^4He$)

To better understand regional mantle degassing in northern Baja California, we compared the results of our regional survey of helium isotope measurements with the mantle velocity structure produced by tomographic studies. Previous studies (Di Luccio et al., 2014; Persaud et al., 2015) have utilized velocity measurements to gain a better insight of the lithospheric structure of Baja California.

Figure 13 is a regional map of Baja California showing our 13 sampling localities superimposed on tomographic data from 25-40 km depth. In this region, areas of low mantle velocity (LVZ) are generally indicative of hot or partially molten mantle, whereas regions of high mantle velocity are reflective of old and dense slab remnants (Wang et al., 2009). To a first order, the regional LVZ is spatially correlated with the $^{3}He/^{4}He$ ratios observed at the surface. A major LVZ is situated between the Main Gulf Escarpment and the Delfin spreading centers in the Gulf of California. The anomaly is centered around Puertecitos, the locality with the highest $^{3}He/^{4}He$ ratio (1.74 R_A) in our study. In addition, three other localities, Punta Estrella, El Volcan, and Plan Nacional Agrario, are also in close proximity to this LVZ. El Volcan and Punta Estrella have similarly high $^{3}He/^{4}He$ ratios (1.31 and 1.13 R_A respectively) with the only exception being PNA, with the lowest $^{3}He/^{4}He$ ratio (0.30 R_A) recorded within this area. One possible explanation for this low ratio in PNA is that it is situated within the San Pedro Mártir mountain range, an area with a crustal thickness of up to 40 km (Lewis et al., 2001). The greater crustal thickness in the area allows for greater mixing between mantle volatiles and crustal/radiogenic materials, resulting in a more diluted helium signature.

Figure 14 is the same regional map of Baja California shown above but with tomographic data from 50 to 90 km depth. Here, we observe that most of the LVZs are found to be generally displaced off axis from the spreading centers in the rift basins. This indicates that the pathway for melt migration is more complex than in an axis-centered LVZ source aligned above a deeper region of mantle melt and likely reflects the spatial evolution of rift segment magamtism. Conversely, the high velocity anomalies beneath

west-central Baja (shown in blue) have been interpreted as a fossil slab now captured by the Pacific plate (Di Luccio et al., 2014).

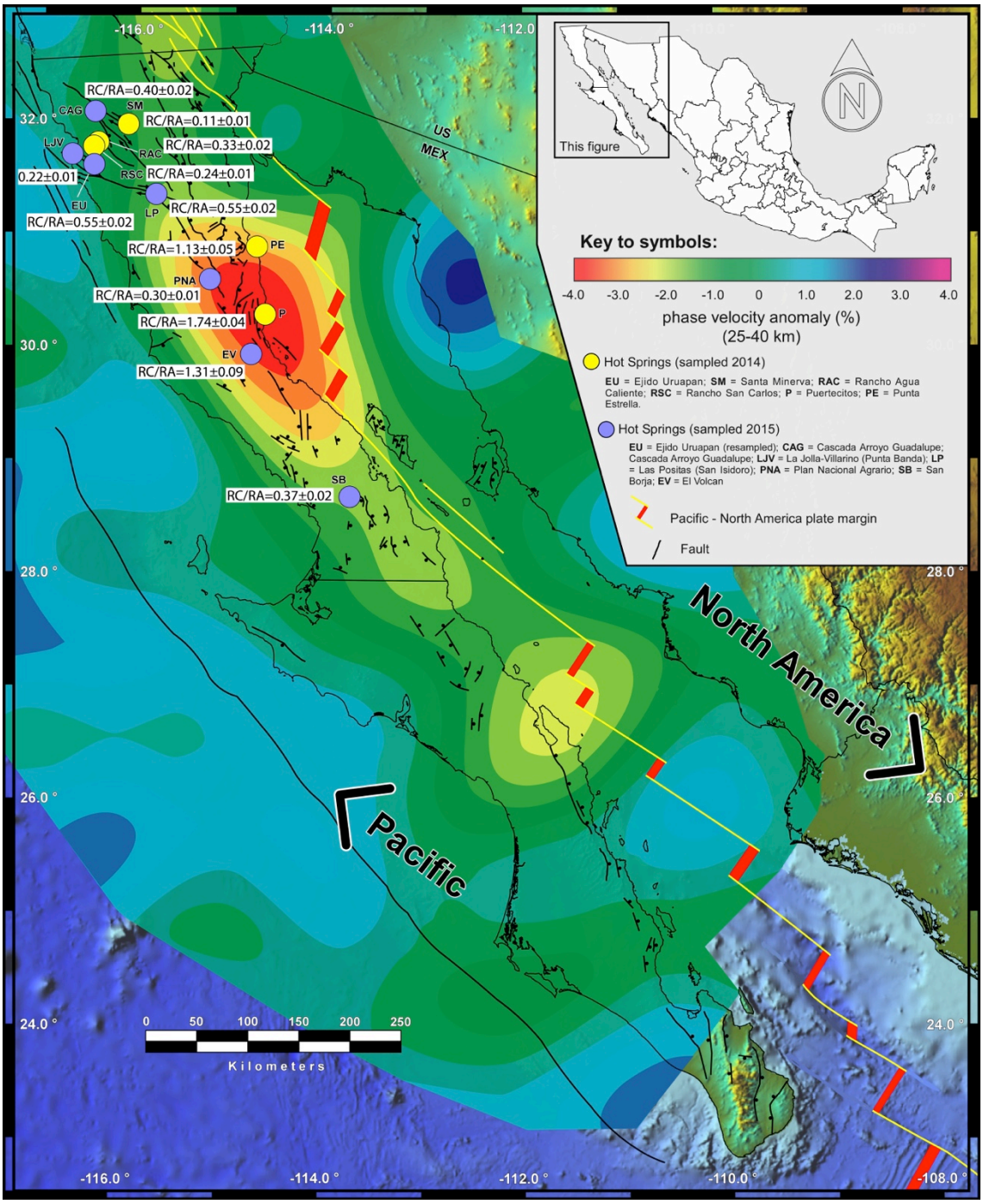

Figure 13: Regional tectonic map of Baja California and the Gulf. Sampling localities are labeled and shown in circles. Velocity anomalies reflect a depth of 25 to 40 km (adapted from Forsyth et al., 2007 and Wang et al., 2009). Figure modified from Spelz et al., 2017.

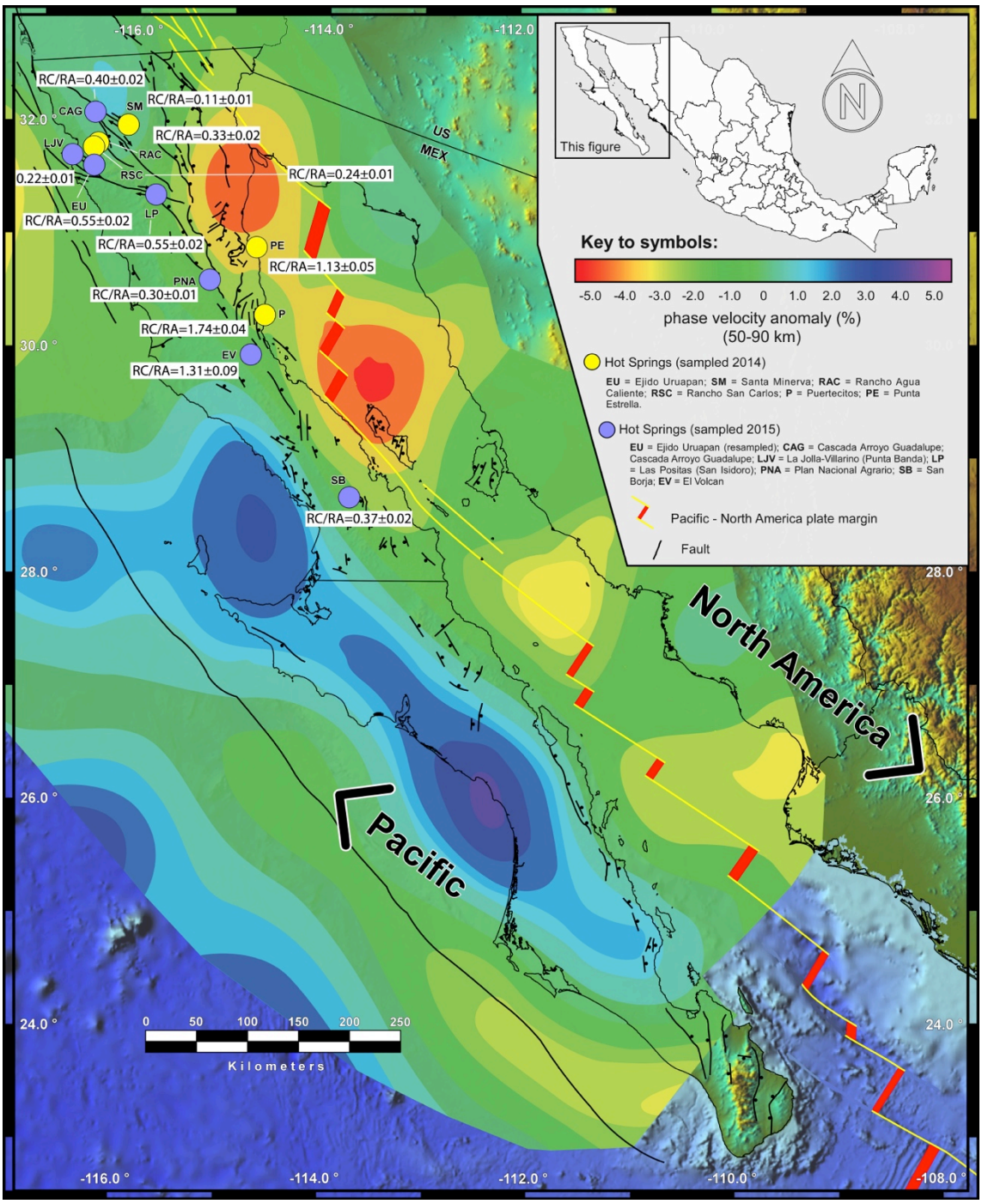

Figure 14: Regional tectonic map of Baja California and the Gulf. Sampling localities are labeled and shown in circles. Velocity anomalies reflect a depth of 50 to 90 km (adapted from Forsyth et al., 2007 and Wang et al., 2009). Figure modified from Spelz et al., 2017.

6. CONCLUSION

This study presents the results of the first detailed helium and carbon isotope investigations of 13 hot springs in northern Baja California. The results reveal that helium isotopes along the northwest region are primarily controlled by the presence of transform faults in the transpeninsular strike-slip province, allowing geothermal fluids to reach the surface through these conduits. The elevated helium isotopes observed along the central and eastern regions may be associated with the proximity of active spreading centers in the Gulf aided by extensional tectonic structures of the Gulf Extensional Province. Helium characteristics reveal that radiogenic crustal input has modified the original sample source characteristics. However, significant mantle volatile contributions (1.1 to 21.4%) are still observable in our samples.

Coupling our helium isotope data with tomography data, we observe a general correlation between high helium isotope ratios and low shear wave velocity anomalies, akin to the results of previous studies focused in the western United States (Newell et al., 2005). These low velocity zones have been interpreted as regions of partial melting and are primarily located near the axis of spreading centers in the rift basins in the Gulf of California. This agreement suggests that low mantle velocity is linked to observed regional degassing as evidenced by ubiquitous mantle helium contribution in spring and groundwater samples.

Determining carbon provenance is limited due to atypical $\delta^{13}C$ values and low $CO_2/^3He$ ratios in our samples. Notably, the L-M-S model does not accurately reflect the carbon origin of our samples due to extensive modification via phase separation and

calcite precipitation. Only the carbon from Puertecitos and El Volcan could be identified (with a degree of uncertainty) in relation to the mantle, sediment, and limestone end-members, with the CO_2 being dominated by limestone input.

The coastal region of Puertecitos and Punta Estrella can be considered as promising geothermal prospects due to their high heat flow and proximity to populated areas. In addition, the offshore Wagner and Consag basins output an average heat flow of 1875 mW/m^2 (Prol-Ledesma et al., 2013), significantly higher than the mean oceanic heat flow. Expanding our study to incorporate more hot springs for analysis, as well as coupling our geochemical data with existing geothermometry data, may prove the feasibility for future development and exploitation of each of the peninsula's geothermal system prospects, and discovery of new prospects that presently are not economically viable using today's technology.

REFERENCES

Andrews, J. (1985). The isotopic composition of radiogenic helium and its use to study groundwater movement in confined aquifers. *Chemical Geology,* 339-351.

Arango-Galván, C., Prol-Ledesma, R.M., Flores-Márquez, E.L., Canet, C., Villanueva Estrada, R.E., 2011. Shallow submarine and subaerial, low-enthalpy hydrothermal manifestations in Punta Banda, Baja California, Mexico Geophysical and geochemical characterization. *Geothermics* 40, 102–111.

Axen, G. (1995). Extensional segmentation of the Main Gulf Escarpment, Mexico and United States. *Geology* v. 23, 515–518.

Ballentine, C.J., van Keken, P.E., Porcelli, D., and Hauri, E.H. (2002). Numerical models, geochemistry and the zero paradox noble gas mantle. Philosophical Transactions of the Royal Society of London. Mathematical, Physical, and Engineering Sciences, 360, 2611 – 2631.

Barry, P., Hilton, D., Fischer, T., Moor, J., Mangasini, F., & Ramirez, C. (2013). Helium and carbon isotope systematics of cold "mazuku" CO2 vents and hydrothermal gases and fluids from Rungwe Volcanic Province, southern Tanzania. *Chemical Geology,* 141-156.

Bruttel, P. A., & Seifert, N. (2007). Analysis of water samples and water constituents with Metrohm instruments. Metrohm Ltd.

Calmus, T., Pallares, C., Maury, R.C., Aguillon-Robles, A., Bellon, H., Benoit, M., and Michaud, F. (2011). Volcanic markers of the post-subduction evolution of Baja California and Sonora, Mexico: Slab tearing versus lithospheric rupture of the Gulf of California. *Pure and Applied Geophysics*, v. 168, 1303–1330.

Castillo, P.R., (2008). Origin of the adakite-high-Nb basalt association and its implications for post-subduction magmatism in Baja California, Mexico. *Geological Society of America Bulletin*, v. 120, 451–462.

Clarke, W.B., Jenkins, W.J., Top, Z. (1976). Determination of tritium by mass spectrometric measurement of He-3. *International Journal of Applied Radiation and Isotopes*, 27, 515–522.

Craig, H., Lupton, J.E., and Horibe Y. (1978). A mantle helium component in circum Pacific volcanic glasses: Hakone, the Marianas and Mt Lassen, In: Alexander, E.C., Ozima, M. (Eds.), Terrestrial Rare Gases. Japan Science Society Press, Tokyo, 3-16.

De Boer, J.Z. (1980). Paleomagnetism of the Quaternary Cerro Prieto, Cater Elegante, and Salton Buttes Volcanic Domes in the northern part of the Gulf of California Rhombochasm. Proceedings 2nd Symposium on the Cerro Prieto Geothermal Field, October 17-19, Mexicali, Mexico, 91–98.

De Leeuw, G.A.M., Hilton, D.R., and Gulec, N., and Mutlu, H. (2010). Regional and temporal variations in $CO_2/^3He$, $^3He/^4He$, and ^{13}C along the North Anatolian Fault Zone, Turkey. *Applied Geochemistry*, v. 25, 524 – 539.

Di Luccio, F., Persaud, P., and Clayton, R.W. (2014). Seismic structure beneath the Gulf of California: a contribution from group velocity measurements. *Geophysical Journal International*, v. 199, 1861 – 1877.

Dickson, A. G., Afghan, J. D., & Anderson, G. C. (2003). Reference materials for oceanic CO_2 analysis: a method for the certification of total alkalinity. *Marine Chemistry*, 80(2), 185-197.

Ellis A.J. Golding, R.M. (1963). The solubility of carbon dioxide above 100°C in water and sodium chloride solutions. *American Journal of Science* 261, 47-60.

Flores-Armenta, M. and Gutierrez-Negrin, L. (2011). Geothermal activity and development in Mexico. Presented at "Short course on geothermal drilling, resource development and power plants." Organized by UNU-GTP and LaGeo, 1 – 12.

Forrest, M.J., Ledesma-Vazquez, J., Ussler III, W., Kulongoski, J.T., Hilton, D.R. and Greene, H.G. (2005). Gas geochemistry of shallow-water hydrothermal activity associated with El Requeson fault zone in Bahia Concepcion, Baja California Sur, Mexico. *Chemical Geology*, v. 224, 82 – 95.

Forsyth, D.W., Wang, Y., and Savage, B. (2007). 3-D Tomography of the Crust and Upper Mantle Beneath the Gulf Extensional Province and Baja California. Abstract presented at Margins Workshop.

Freeze, R.A. and J.A. Cherry. (1979). *Groundwater*. Prentice-Hall, Inc. Englewood Cliffs, NJ.

Fritz, S. (1994). A Survey of Charge-Balance Errors on Published Analyses of Potable Ground and Surface Waters. *Ground Water,* 539-546.

Gastil, R.G., Phillips, R.P., and Allison, E.C. (1975). Reconnaissance geology of the State of Baja California. *Geological Society of America*, Memoir 140.

Giggenbach, W.F., Sano, Y., and Wakita, H. (1993) Isotopic composition of helium, and CO2 and CH4 contents in gases produced along the New Zealand part of a convergent plate boundary. *Geochimica et Cosmochimica Acta*, v. 57, 3427 – 3455.

Graham, D. W. (2002). Noble gas isotope geochemistry of mid-ocean ridge and ocean island basalts: Characterization of mantle source reservoirs. *Reviews in Mineralogy and Geochemistry*, 47(1), 247-3.

Gulec, N., Hilton, D.R., Mutlu, H., 2002. Helium isotope variation in Turkey: relationship to tectonics, volcanism and recent seismic activities. Chemical Geology 187, 129–142.

Gutierrez-Negrin, L. and Quijano-Leon, J. (2005). Update of Geothermics in Mexico. *Proceedings World Geothermal Congress*, 1 – 10.

Hilton, D. R., Fischer, T. P. and Marty, B. (2002) Noble gases and volatile recycling at subduction zones. Noble Gases in Cosmochemistry and Geochemistry (Porcelli, D., Ballentine, C. J. and Wieler, R., eds.), *Mineralogical Society of America*, Washington, D.C.

Hilton, D.R. (1996). The helium and carbon isotope systematics of a continental geothermal system: result from monitoring studies at Long Valley caldera (California, U.S.A.). *Chemical Geology* 127, 269–295.

Hilton, D.R. (2007). Perspectives in Geochemistry: The leaking mantle. *Science* 318, 1389 – 1390.

Hilton, D.R. and Porcelli, D. (2003). Noble gases as mantle tracers. In: The Mantle and Core (ed. Carlson, R.W.) Vol. 2 Treatise on Geochemistry (eds. Holland, H.D. and Turekian, K.K.), Elsevier-Pergamon, Oxford, UK, 277 – 318.

Hiscock, K., & Bense, V. (2014). *Hydrogeology: principles and practice*. John Wiley & Sons.

Kennedy, B.M., Kharaka, Y.K., Evans W.C., Ellwood, A., DePaolo, D.J., Thordsen, J., Ambats, G., and Mariner, R.H. (1997). Mantle Fluids in the San Andreas Fault System, California. *Science*, v. 278, 1278 – 1281.

Kulongoski, J. T., & Hilton, D. R. (2002). A quadrupole‐based mass spectrometric system for the determination of noble gas abundances in fluids. *Geochemistry, Geophysics, Geosystems*, 3(6), 1-1.

Kulongoski, J. T., D. R. Hilton, and J.A. Izbicki. (2005). Source and movement of helium in the eastern Morongo groundwater basin: the influence of regional tectonics on crustal and mantle helium fluxes. *Geochimica et Cosmochimica Acta,* 69: 3857-3872.
Kulongoski, J.T. and Hilton, D.R. (2011). Applications of groundwater helium. In: M. Baskaran (Editor), *Handbook of Environmental Isotope Geochemistry*. Springer- Verlag, pp. 285-304.

Kulongoski, J.T., Hilton, D.R., Barry, P.H., Esser, B.K., Hillegonds, D., and Belitz, K. (2013). Volatile fluxes through the Big Bend section of the San Andreas Fault, California: Helium and carbon-dioxide systematics. *Chemical Geology*, v. 339, 92 – 102.

Lewis, J.L., Day, S.M., Magistrale, H., Castro, R.R., Astiz, L., Rebollar, C., Eakins, J., Vernon, F.L., and Brune, J.N. (2001). Crustal thickness of the Peninsular Ranges andn Gulf Extensional Province in the Californias. *Journal of Geophysical Research*, v. 106, 13599–13611.

Lindsay, L. and Hample, W.G. (1998). *Geology and Geothermal Resources of the Imperial and Mexicali Valleys*. San Diego Association of Geologists. San Diego, CA.

Lollar, S.B., Ballentine, C.J., O'Nions, R.K., (1997). The fate of mantle-derived carbon in a continental sedimentary basin: Integration of C/He relationships and stable isotope signatures. *Geochimica et Cosmochimica Acta*, v. 61, 2295 – 2307.

Lonsdale, P. (1989). Geology and tectonic history of the Gulf of California. The Geology of North America v. N, The Eastern Pacific Ocean and Hawaii. *Geological Society of America*, 499–521.

Luhr, J.F., Aranda-Gomez, J.J., Housh, T.B. (1995). San Quintin Volcanic Field, Baja California Norte, Mexico: Geology, Petrology, and Geochemistry. *Journal of Geophysical Research*, v. 100, 10353–10380.

Martin-Barajas, A., Stock, J.M., Layer, P., Hausback, B., Renne, P., and Lopez-Martinez, M. (1995). Arc-rift transition volcanism in the Puertecitos Volcanic Province, northeastern Baja California, Mexico. *Geological Society of America Bulletin*, v. 107, 407–424.

Marty, B., & Jambon, A. (1987). $C/^{3}He$ in volatile fluxes from the Solid Earth: Implications for carbon geodynamics. *Earth and Planetary Science Letters*, 83(1), 16-26.

Marty, B., Jambon, A., & Sano, Y. (1989). Helium isotopes and CO2 in volcanic gases of Japan. *Chemical Geology,* 25-40.

McLing T. L., Smith R. W., Johnson T. M. (2001) Chemical characteristics of thermal water beneath the eastern Snake River Plain, *Spec. Pap. Geol. Soc. Am.,* 353, 205–211.

Michaud, F., Royer, J.Y., Bourgois, J., Dyment, J., Calmus, T., Bandy, W., Sosson, M., Mortera-Gutierrez, C., Sichler, B., Rebolledo-Viera, M., and Pontoise, B. (2006). Ocean-ridge subduction vs. slab breakoff: Plate tectonic evolution along the Baja California Sur continental margin since 15 Ma, *Geology* v. 34, 13–16.

Negrete-Aranda, R., Canon-Tapia, E., Brandle, J.L., Ortega-Rivera, M.A., Lee, J.K.W., Spelz, R.M., and Hinijosa-Corona, A. (2010). Regional orientation of tectonic stress

expressed by post-subduction high-magnesium volcanism in northern Baja California, Mexico: Tectonics and volcanism of San Borja volcanic field. *Journal of Volcanology and Geothermal Research*, v. 192, 97–115.

O'Nions, R. K., & Oxburgh, E. R. (1988). Helium, volatile fluxes and the development of continental crust. *Earth and Planetary Science Letters*, 90(3), 331-34.

Ozima, M., & Podosek, F. A. (2002). *Noble gas geochemistry*. Cambridge University Press.

Pallares, C., Bellon, H., Benoit, M., Maury, R.C., Aguillon-Robles, A., Calmus, T., and Cotten, J. (2008). Temporal geochemical evolution of Neogene volcanism in northern Baja California: insights on the origin of post-subduction magnesian andesites. *Lithos*, v. 105, 162–180.

Parkhurst, D.L., and Appelo, C.A.J. (2013). Description of input and examples for PHREEQC version 3—A computer program for speciation, batch-reaction, one-dimensional transport, and inverse geochemical calculations: *U.S. Geological Survey Techniques and Methods*.

Paz Moreno, F.A. and Demant, A. (1999). The recent Isla San Luis volcanic centre: petrology of a rift-related volcanic suite in the northern Gulf of California, Mexico. *Journal of Volcanology and Geothermal Research*, v. 93, 31–52.

Pérez-Flores, M.A., Suárez Vidal, F., Gallardo Delgado, L.A., González Fernández, A., Vázquez, R., 2004. Structural pattern of the Todos Santos Coastal plain, based on geophysical data. Cienc. Marinas 30, 349–364.

Persaud, P., Di Luccio, F., and Clayton, R.W. (2015). Rayleigh wave dispersion measurements reveal low-velocity zones beneath the new crust in the Gulf of California. *Geophysical Research Letters*, v. 42, 1766 – 1774.

Piper, A.M. (1944). A graphic procedure in the geochemical interpretation of water analyses *Transactions of the American Geophysical*, 25, 914-923.

Prol-Ledesma, R.M., Torres-Vera, M.A., Rodolfo-Metalpa, R., Ángeles, C., Lechuga Deveze, C.H., Villanueva-Estrada, R.E., Shumilin, E., Robinson, C. (2013). High heat flow and ocean acidification at a nascent rift in the northern Gulf of California. *Nature Communications*, v. 1388, 1 – 7.

Ray, M.C., Hilton, D.R., Munoz, J., Fischer, T.P., and Shaw, A.M. (2009). The effects of volatile recycling, degassing and crustal contamination on the helium and carbon geochemistry of hydrothermal fluids from the Southern Volcanic Zone of Chile. *Chemical Geology*, v. 266, 38 – 49.

Sano, Y., Marty, B. (1995). Origin of carbon in fumarolic gas from island arcs. *Chemical Geology* 119, 265–274.

Sano, Y., Nakamura, Y., Wakita, H., Urabe, A., Tominaga, Y. (1984). 3He emission related to volcanic activity. *Science* 224, 150–151.
Seiler, C., Fletcher, J.M., Quigley, M.C., Gleadow, A.J.W., and Kohn, B.P. (2010). Neogene structural evolution of the Sierra San Felipe, Baja California: Evidence for proto-gulf transtension in the Gulf Extensional Province? *Tectonophysics*, v. 488, 87–109.

Spane F. A., Webber W. D. (1995) Hydrochemistry and hydrogeologic conditions within the Hanford Site upper basalt confined aquifer system, *PNL*-10817, Pac. Northw. Natl. Lab., Richland, Wash.

Spelz, R.M., Negrete-Aranda, R., Hilton, D.R., Virrueta, C., Téllez, M., Lupton, J.E., Evans, L.J., Clague, D.A., Zierenberg, R.A., Neumann, F. (2017). *Mapping mantle-melting anomalies in Baja California: a combined subaereal-submarine noble gas geochemistry new data set*. Abstract T22B-03 presented at 2017 Fall Meeting, AGU, New Orleans, LA, 11-15 December.

Suarez-Vidal, F., Munguia-Orozco, L., Gonzalez-Escobar, M., Gonzalez-Garcia, J., and Glowacka, E. (2007). Surface rupture of the Morelia fault near the Cerro Prieto geothermal field, Mexicali, Baja California, Mexico, during the M 5.4 Earthquake of 24 May 2006. *Seismological Research Letters*, v. 78, 394–399.

Tian, L., Paterno, C.R., Lonsdale, P.F., Hahm, D., and Hilton, D.R. (2011). Petrology and Sr-Nd-Pb-He isotope Geochemistry of postspreading lavas on fossil spreading axes off Baja California Sur, Mexico. *Geochemistry, Geophysics, Geosystems*, 12(2), 1-22.

Trick, J. K., Stuart, M., & Reeder, S. (2008). Contaminated groundwater sampling and quality control of water analyses. *Environmental geochemistry site characterization, data analysis and case histories. Elsevier, London*, 29-57.

U.S. Environmental Protection Agency. (1993). Method 300.0 Determination of inorganic anions by ion chromatography, rev 2.1: Cincinnati, Ohio, *Environmental Monitoring and Support Laboratory*, p.13.

Umhoefer, P.J., Dorsey, R.J., Willsey, S., Mayer, L., and Renne, P. (2001). Stratigraphy and geochronology of the Comondu Group near Loreto, Baja California sur, Mexico. *Sedimentary Geology*, v. 144, 125–147.

Vidal, F.V., Welhan, J.A., and Vidal, V.M.V. (1982). Stable isotopes of helium, nitrogen and carbon in a coastal submarine hydrothermal system. *Journal of Volcanology and Geothermal Research*, v. 12, 101 – 110.

Vidal, V.M.V., Vidal, F.V., Isaacs, J.D. (1981). Coastal submarine hydrothermal activity off northern Baja California: Evolutionary history and isotope geochemistry. *Journal of Geophysical Research*, v. 86, 9451–9468.

Vogel, J.C., Grootes, P.M., Mook, W.G. (1970). Isotope fractionation between gaseous and dissolved carbon dioxide. *Zeitschrift für Physik* 230, 255–258.

Wallace, R.E. (1990). *The San Andreas Fault System, California*. Washington, DC: US Government Printing Office. US Geological Survey Professional Paper 1515.
Wang, Y., Forsyth, D.W., and Savage, B. (2009). Convective upwelling in the mantle beneath the Gulf of California. *Nature*, v. 462, 499 – 501.

Weiss, R. F. (1968), Piggyback sampler for dissolved gas studies on sealed water samples, *Deep Sea Res*., 15, 695-699.

Weiss, R. F. (1971). Solubility of helium and neon in water and seawater. *Journal of Chemical & Engineering Data*, 16(2), 235-241.

Welhan, J.A., Poreda, R.J., Rison, W., and Craig, H., (1988). Helium isotopes in geothermal and volcanic gases of the western United States, regional variability and magmatic origin. *Journal of Volcanology and Geothermal Research*, v. 34, 185 – 199.